



Article

Rice Height Estimation with Multi-Baseline PolInSAR Data and Optimal Detection Baseline Combination Analysis

Bolin Zhang ^{1,2}, Kun Li ^{1,2,3,*}, Fengli Zhang ^{1,2} , Yun Shao ^{1,2,3}, Duo Wang ⁴ and Linjiang Lou ⁵

¹ Aerospace Information Research Institute, Chinese Academy of Sciences, Beijing 100101, China; zhangbolin21@mails.ucas.ac.cn (B.Z.); zhangfl@aircas.ac.cn (F.Z.); shaoyun@aircas.ac.cn (Y.S.)

² College of Resources and Environment, University of Chinese Academy of Sciences, Beijing 100049, China

³ Laboratory of Target Microwave Properties (LAMP), Deqing Academy of Satellite Applications, Huzhou 313200, China

⁴ State Geospatial Information Center, Beijing 100070, China; wangd@sgic.net.cn

⁵ Land Satellite Remote Sensing Application Center, MNR, Beijing 100048, China; llj910808@hotmail.com

* Correspondence: likun201032@aircas.ac.cn

Abstract: Rice is a primary food source, and height is a crucial parameter affecting its growth status. Consequently, high-precision, real-time monitoring of quantitative changes in crop height are required for improved crop production. Polarimetric interferometric SAR (PolInSAR) has both polarization and interferometric observation capabilities. Due to the short height of crops and rapid growth changes, the large spatial and short temporal baselines of PolInSAR data are essential for effective crop height inversion; however, relevant satellite-borne SAR and airborne SAR data are currently limited. This study presents a PolInSAR rice height inversion algorithm that uses the oriented volume over ground (OVoG) mode with PolInSAR 0-time and controllable spatial baseline data from a LAMP microwave anechoic chamber. Exploiting the advantages of microwave anechoic chamber measurement data, which includes continuous frequency bands, multiple baselines, and varied incidence angles, the influences of incident angles, baseline length, number of baselines, and baseline combinations are assessed. The highest accuracy rice plant height inversion has a root mean square deviation (RMSE) of 0.1093 m and is achieved with an incidence angle of 35–55°, baseline length of 0.25°, and three to four baselines. Furthermore, an imaging geometric equivalence analysis provides reliable foundation data to guide research into new earth observation SAR systems. The results indicate that, under simulated observations from the GF3 satellite at an altitude of 755 km, the optimal spatial baseline ranges for various frequency bands are as follows: L-band: 10.93–42.59 km; S-band: 4.10–15.97 km; C-band: 2.48–9.64 km; X-band: 1.36–5.32 km; Ku-band: 0.87–3.40 km. Notably, the measurement modes corresponding to the C, X, and Ku bands are ultimately identified as the most suitable for PolInSAR rice height inversion.

Keywords: rice height; polarimetric synthetic aperture radar interferometry (PolInSAR); Laboratory of Target Microwave Properties (LAMP); parameter retrieval



Citation: Zhang, B.; Li, K.; Zhang, F.; Shao, Y.; Wang, D.; Lou, L. Rice Height Estimation with Multi-Baseline PolInSAR Data and Optimal Detection Baseline Combination Analysis. *Remote Sens.* **2024**, *16*, 358. <https://doi.org/10.3390/rs16020358>

Academic Editor: Deodato Tapete

Received: 29 November 2023

Revised: 12 January 2024

Accepted: 14 January 2024

Published: 16 January 2024



Copyright: © 2024 by the authors. Licensee MDPI, Basel, Switzerland. This article is an open access article distributed under the terms and conditions of the Creative Commons Attribution (CC BY) license (<https://creativecommons.org/licenses/by/4.0/>).

1. Introduction

Rice is one of the world's three major food crops and a primary food source for over half the global population. China boasts a cultivation area of approximately 29.92 million hectares, ranking first in the world in terms of annual rice production. Plant height is a comprehensive reflection of the intrinsic characteristics of rice plants, as well as environmental factors such as climate, hydrology, and soil, and is an important basis for monitoring growth, estimating yield, and evaluating greenhouse gas emissions [1]. Therefore, the accurate and timely acquisition of rice plant height across extensive areas is of great significance for safeguarding national food security, promoting the reduction of agricultural emissions and efficiency enhancement, advancing carbon sequestration, and contributing to the development of a national dual carbon strategy.

The conventional approach for determining rice height primarily relies on field observations, which are time-consuming and labor-intensive processes with limited coverage and inadequate timelines. Remote sensing technology is an important means of Earth observation and offers advantages such as large-scale synchronous observation, short revisit periods, and a high level of timeliness. Furthermore, it is already widely utilized for crop monitoring and parameter acquisition. Rice is frequently grown in hot and humid environments that experience cloudy and rainy weather during the growing season, and this results in challenges regarding optical remote sensing data acquisition [2,3]. Synthetic aperture radar (SAR) can uniquely penetrate clouds, allowing for observations under most weather conditions. This is advantageous for the inversion of rice parameters in cloudy and rainy weather during the growing season [4,5].

The main methods for SAR vegetation height monitoring are based on radiative transfer modeling, Interferometric Synthetic Aperture Radar (InSAR)-based Digital Elevation Model (DEM) differencing, Polarimetric Synthetic Aperture Radar Interferometry (PolInSAR)-based complex coherence differencing, and model-solving algorithms [6,7]. The method based on radiative transfer theory uses the radiative transfer equation to model the quantitative relationship between radar backscattering coefficients and plant structure (plant height), dielectric properties, and thus plant height inversion [8]. The advantage of this method lies in its solid physical foundation; however, it suffers from the drawback of having a plethora of model parameters, resulting in lower computational accuracy. The InSAR-based DEM difference method obtains phase difference information from two or more images of different orbits, calculates the digital surface model (DSM), and obtains the vegetation height by differentiating the DSM from the external DEM data. The accuracy of this method is affected by the heterogeneity of the vegetation as well as the accuracy of the external DEM [9,10]. PolInSAR combines the characteristics of polarimetric SAR, which is sensitive to the shape and direction of scatterers, and the characteristics of InSAR, which is sensitive to the spatial distribution of scatterers [11]. Furthermore, it establishes a quantitative relationship for the multi-polarized phase interference using a multichannel polarization synthesis technique, which can significantly improve the signal-to-noise ratio of the interferometric phase and improve the accuracy of the inversion of the ground height and parameters [12–14]. The PolInSAR complex coherence difference method relies on the phase differences associated with different scattering mechanisms to estimate vegetation height. However, the reliability of this method is limited by the penetration depth of the microwave signals. Real surface information cannot be obtained when the penetration depth is shallow [15]. The PolInSAR model-based inversion approach abstracts vegetated scenes into two layers: vegetation and ground. This replaces complex vegetation structure functions with empirical models containing a limited number of unknown parameters, thereby simplifying the structural functions. Model-based inversion methods are computationally efficient and can produce higher levels of inversion accuracy. Among these, the random volume over ground (RVoG) and oriented volume over ground (OVoG) models are the most widely applied for PolInSAR vegetation height retrieval [16–18]. Many studies on agricultural vegetation suggest that the orientation effects introduced by stalk shape may result in polarization-dependent propagation through the canopy [19]. In such cases, considering the propagation direction makes the OVoG model more suitable for simulating crop height. The main constraint of using such a model is the large number of structural parameters with respect to the available measurements. Solving the numerous parameters of the OVoG model using a single baseline often leads to ill-conditioned solutions. Therefore, the utilization of prior knowledge assumptions or the extension of the observation space dimension via multi-baseline data is required.

Currently, PolInSAR vegetation height inversion primarily uses satellite-based SAR, airborne SAR, and microwave anechoic chamber data. Spaceborne SAR data from satellites such as Sentinel-1, GF-3, and TanDEM/TerraSAR-X can also be utilized to provide the PolInSAR data. However, these satellites have rarely incorporated PolInSAR crop monitoring into their design and operation and are typically utilized to assess forest height

inversion. Consequently, there is a scarcity of baseline data that are specifically sensitive to crop structure. Noelia et al. [18] present a modified PolInSAR inversion methodology based on the operator TrCoh and validated it with reference data obtained from TanDEM-X data in the Spanish rice zone, and the root mean square error of the improved method was improved by 7 cm compared to the traditional method. Lopez Sanchez et al. [20] inverted rice heights in Spain and Turkey using time-series large baseline PolInSAR data taken by TanDEM-X from April to September 2015, with a root mean square error (RMSE) in the range of 10–20 cm; however, the estimates were distorted since the initial rice growth heights were <40 cm owing to the low sensitivity for short plants when using PolInSAR data. Airborne SAR data offers a higher resolution than Spaceborne SAR data and can provide data with various baselines and incidence angles. Notable platforms include E-SAR (Germany), F-SAR (Germany), UAVSAR (USA), and RAMSES (France) [21]. Lopez-Sanchez et al. inverted the heights of crops such as oilseed rape, maize, wheat, barley, and sugar beet based on the RVoG model using fully polarimetric SAR three baseline data acquired by the German Aerospace Center's (DLR) airborne synthetic aperture radar (E-SAR) at DLR. The accuracy of height estimation for maize and rape is about 10%. However, there was a notable overestimation of sugar beets owing to the limited availability of baselines [22]. Pichierri et al. [23] investigated the impact of vertical wavenumbers on the multi-baseline height inversion algorithm performance based on simulated data and validated it in wheat, barley, maize, and oilseed rape plots using X-, L-, and C-band data from the airborne F-SAR in the Wallerfing region of Germany provided by the DLR; the height estimation RMSE of maize and oilseed rape in the L-band was only 10%, while that for wheat and barley in the X-band was approximately 24%. Airborne SAR data can provide more flexible baseline and band configurations, which are limited by the complexity of the operation and data processing and relatively high acquisition costs. Ground-based and indoor microwave laboratories (such as the EMSL laboratory in Europe) can measure the backscattering coefficients of features at multiple frequencies, incidence angles, and time-domain responses, providing a rich database for model and algorithm studies. Li et al. [24] analyzed the images for frequency and baseline length using a rice inversion algorithm based on the data from the LAMP laboratory and found that a baseline of 0.5° , within the frequency range of 2.5 to 4.7 GHz, provided a more accurate rice height inversion when compared with other frequencies. Ballester-Berman et al. [21] developed a retrieval algorithm for crop height inversion based on maize and rice data measured from the EMSL data, with a maximum error of 10 cm for terrain estimation, 30 cm for vegetation height estimation, and some baseline configurations have errors < 15 cm.

To address the issue of insufficient multi-baseline PolInSAR data, this paper conducted rice height inversion using the OVoG model, utilizing PolInSAR data obtained from the Laboratory of Microwave Properties (LAMP). LAMP serves as a scientific microwave anechoic chamber for land-target microwave characteristic measurement and simulation. Exploiting the versatile and controllable features of the microwave anechoic chamber, we obtained measurement data with continuous frequency bands, multiple baselines, and multiple incidence angles. A comprehensive investigation was conducted to analyze the impact patterns of factors such as frequency bands, baseline length, number of baselines, baseline combinations, and incidence angles on the inversion of rice plant height, aiming to provide insights into the optimal detection mode for rice height inversion. Furthermore, considering the imaging characteristics of the LAMP anechoic chamber, we explored the equivalence between microwave anechoic chamber measurement data and satellite data. This exploration led to the identification of the optimal detection mode for PolInSAR satellite rice height inversion based on microwave anechoic chamber results. This study furnishes reliable data support for the design and preliminary validation of future Synthetic Aperture Radar (SAR) satellite polarization interference measurement capabilities.

2. Materials and Methods

2.1. LAMP Data Set

The PolInSAR data used in this study were obtained from a microwave anechoic chamber for measuring and simulating the microwave characteristics of land targets. The microwave anechoic chamber consisted of a pure, interference-free microwave test environment in a 24 m (L) × 24 m (W) × 17 m (H) space (Figure 1). The radar signal source for LAMP comes from the N5222A vector network analyzer. The radar signal is transmitted and received through four full-polarized antennas, including two QR800 antennas for transmitting and receiving radar signals at the frequency of 0.8–6 GHz and two QR6000 antennas for transmitting and receiving radar signals at the frequency of the 6–18 GHz measurement band. The precision orbit system of the microwave anechoic chamber has a positioning accuracy of 0.1 mm and an orientation accuracy of 0.01°, which can achieve high-precision and quantitative control of the relative position and movement between the antenna and the target to be tested. The high-precision RF measurement system of the microwave anechoic chamber has a dynamic range of up to 100 dB and a sensitivity greater than −60 dBsm, which is capable of obtaining continuous microwave spectral characteristics of the target to be measured in the frequency range of 0.8–18 GHz. This microwave anechoic chamber enables the complete processing of microwave characterization, encompassing sample preparation, scene simulation, and simulated SAR imaging across a multitude of parameters for the different microwave target characteristic measurements, such as “component target-scenario”. It provides comprehensive measurements of the microwave characteristics, including multiband data, full polarization (HH/HV/VH/VV), multi-angle (0–90°), and omnidirectional (0–360°) measurements, as well as SAR imaging simulations. The microwave anechoic chamber can simulate a wide range of SAR remote sensing imaging modes, from conventional (such as SpotLight, StripMap, and ISAR) to complex (such as PolSAR, InSAR, and PolInSAR). It achieves a maximum spatial resolution of 1 cm [25].

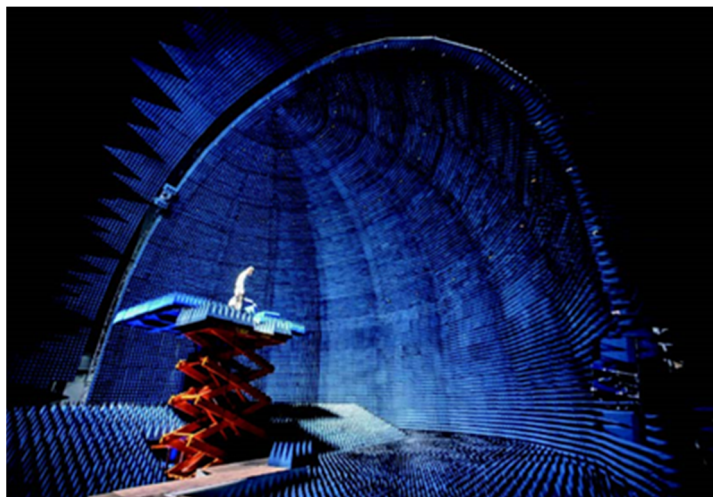


Figure 1. Inside view of the microwave anechoic chamber.

When the rice scene was constructed by transplanting rice plants from the field into sample boxes, the plant distribution and density in real rice fields were strictly followed; the size of the observation scene was 1.2 m × 1.8 m. The rice variety was japonica, the climatic period was milky ripening, and the average plant height was 1.0 m. After constructing the rice scene, wave-absorbing cotton was placed around the scene to ensure that all echo signals came from the rice scene being tested (Figure 2). In addition, the experimental measurements, microwave anechoic chamber temperature, humidity, wind speed, and other parameters were set to be consistent with the actual growth environment of rice.

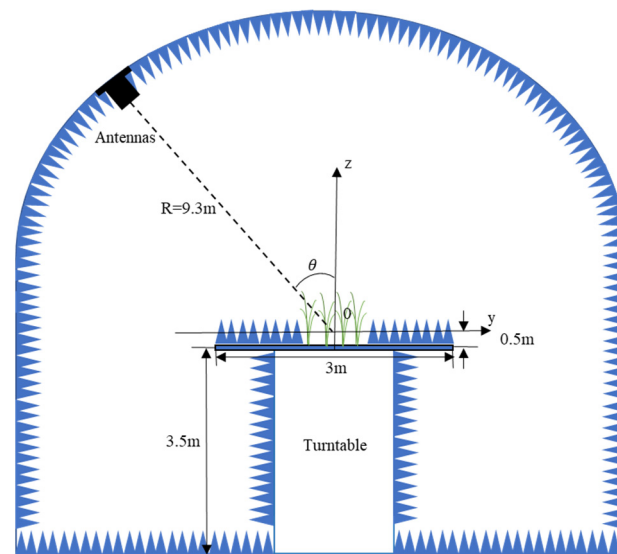


Figure 2. Rice field scene layout (front view) in the LAMP microwave anechoic chamber.

After the rice scene was constructed, the LAMP microwave anechoic chamber was used to obtain PolInSAR data in the continuous frequency band of 0.8–18 GHz, at different central incidence angles of 15–75°, and at different baseline conditions of 0.25–2.0°, with the specific parameters shown in Table 1.

Table 1. Parameters of the scattering measurement data.

Angle of incidence (°)	15	25	35	45	55	65	75	
Baseline length (°)	0.25	0.5	0.75	1.0	1.25	1.5	1.75	2.0
Frequency (GHz)	0.8–7.0			6.0–18				

After acquiring the PolInSAR data using the LAMP microwave anechoic chamber, the data were reprocessed (Figure 3). First, the distance gate limitation and empty-house measurements were used to further remove the influence of clutter signals. Polarization calibration processing was performed on the measurement data to compensate for errors caused by the measurement system. Finally, the measurement data were processed by focusing on imaging to obtain PolInSAR data pairs, and this functioned as data preparation for the subsequent PolInSAR rice plant height inversion.

2.2. OVoG Inversion Scheme

2.2.1. OVoG Model

It is crucial to correlate the observations of different polarization interferometric complex coherence coefficients with the parameters to be inverted and to characterize the vegetation scene as realistically as possible when using PolInSAR to invert the vertical structural vegetation parameters. The OVoG model determines the scattering process for a vegetation scene as a joint action of the vegetation and surface scattering layers, whose scattering characteristics depend on inhomogeneous particle orientation distributions in the vegetation layer [13,17]. In this model, the upper and lower layers represent vegetation and underlying ground surfaces, respectively. The height of the vegetation layer (denoted as h_v) is associated with a single point in the vertical coordinate for the scattering that originates from the ground. Meanwhile, scattering from the vegetation layers is described by the scattering function $f(z)$.

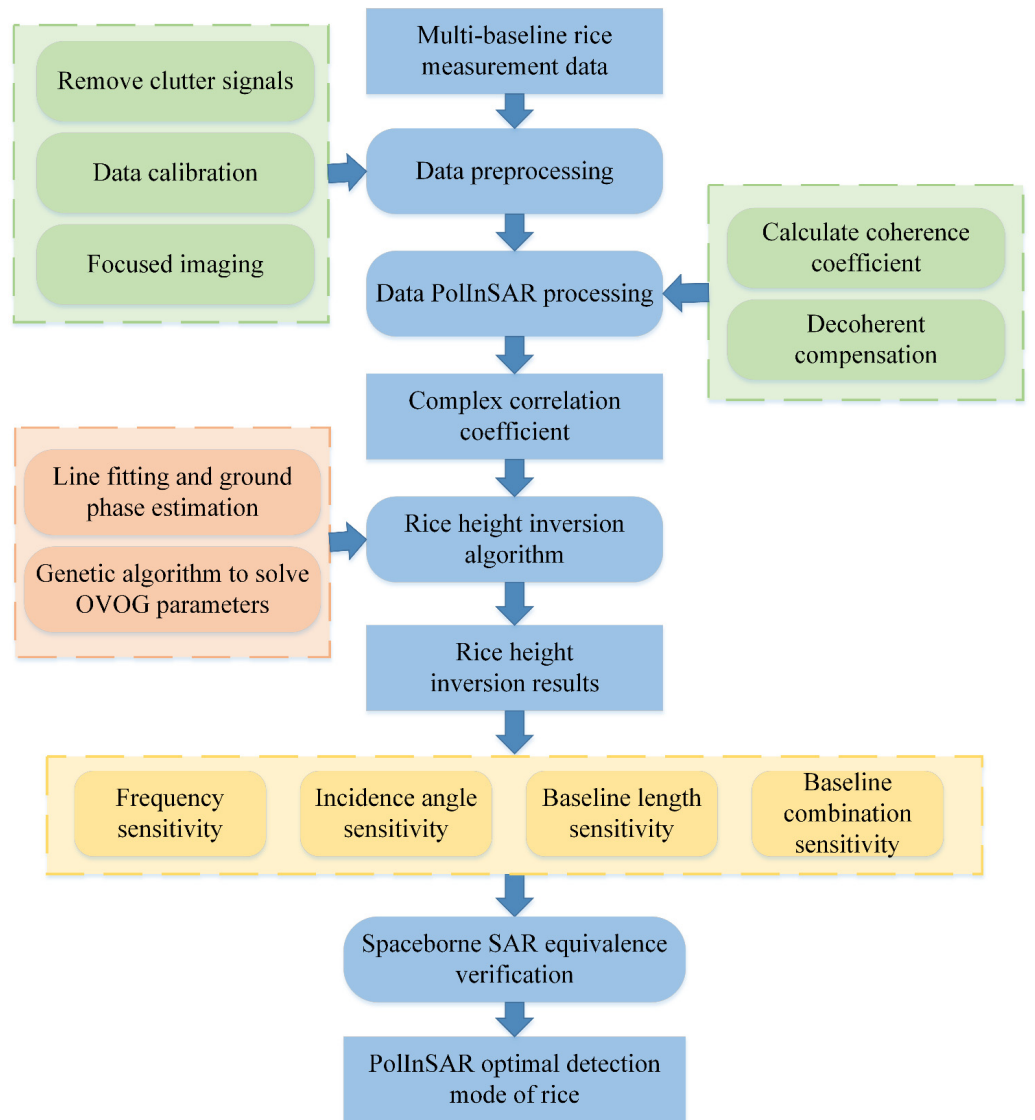


Figure 3. Flowchart of data processing and analysis.

The interference coherence matrix $[\Omega_{\text{OVoG}}]$ and polarization coherence matrix $[T_{\text{OVoG}}]$ of OVoG can be represented by the contributions from the ground and vegetation layers, denoted as m_S and m_V , as follows:

$$[\Omega_{\text{OVoG}}] = m_S[\Omega_S] + m_V[\Omega_{\text{OV}}] \quad (1)$$

$$[T_{\text{OVoG}}] = m_S[T_S] + m_V[T_{\text{OV}}] \quad (2)$$

where $[\Omega_S]$ and $[T_S]$ represents the ground interferometric coherence matrix and the polarization coherence matrix; $[\Omega_{\text{OV}}]$ and $[T_{\text{OV}}]$ represent the volume interferometric coherence matrix and polarization coherence matrix, respectively.

Assuming polarimetric stationarity and equal polarization at both baseline ends, the interference coherence $\gamma_{\text{OVoG}}(\vec{\omega})$ can be expressed as follows:

$$\gamma_{\text{OVoG}}(\vec{\omega}) = \frac{\vec{\omega}^T [\Omega_{\text{OVoG}}] \vec{\omega}}{\vec{\omega}^T [T_{\text{OVoG}}] \vec{\omega}} = e^{i\phi_0} \frac{\gamma_{\text{OV}}(\vec{\omega}) + \mu(\vec{\omega})}{1 + \mu(\vec{\omega})} \quad (3)$$

where the normalized projection vectors $\vec{\omega}$ correspond to the co-polarizations and the cross-polarization in the eigenpolarization basis; ϕ_0 represents the surface phase, and i is the imaginary part of the negative. Interference coherence can also be derived from the ground-to-volume scattering ratio μ and volume decorrelation γ_{OV} [26], as follows:

$$\mu(\vec{\omega}) = \frac{(\sigma_a(\vec{\omega}) + \sigma_b(\vec{\omega}))}{\cos \theta (e^{(\sigma_a(\vec{\omega}) + \sigma_b(\vec{\omega}))h_V / \cos \theta} - 1)} \frac{\vec{\omega}^T [T'_S] \vec{\omega}}{\vec{\omega}^T [T'_{OV}] \vec{\omega}} \geq 0 \quad (4)$$

$$\gamma_{OV}(\vec{\omega}) = \frac{\int_0^{h_V} e^{\frac{(\sigma_a(\vec{\omega}) + \sigma_b(\vec{\omega}))}{\cos \theta} z} e^{iK_z z} dz}{\int_0^{h_V} e^{\frac{(\sigma_a(\vec{\omega}) + \sigma_b(\vec{\omega}))}{\cos \theta} z} dz} \quad (5)$$

where θ represents the incidence angle and the vegetation layer is considered an anisotropic medium in the OVOG model; σ_a and σ_b denote the extinction coefficients for horizontal and vertical polarization, respectively; and k_z is the vertical wave number for the data in the PolInSAR imaging geometry conditions of the LAMP microwave anechoic chamber [27] which can be expressed as follows:

$$k_z = \frac{4\pi f \Delta \theta}{c \sin \theta_c} \quad (6)$$

where f denotes the frequency; c is the speed of light; and θ_c is the average of the incident angles of the interfering primary and secondary images, and $\Delta \theta$ denotes the difference in incidence angle between the primary and secondary images.

2.2.2. Rice Height Inversion Algorithm Based on the OVoG Model

A workflow diagram of the rice height inversion algorithm based on the OVoG model is shown in Figure 3.

The OVoG model contains seven unknowns: ground-phase ϕ_0 , vegetation height h_V , extinction of the two characteristic polarizations σ_a with σ_b , and the ground-to-volume scattering ratio of the three polarization channels μ_{HH} , μ_{HV} , and μ_{VV} . Full-polarimetric single-baseline SAR acquisition acquires the complex coherence of the two co-polarization and cross-polarization channels and can provide three complex coherence values containing real and imaginary parts. If only one baseline is used for the solution without solving the surface phase or simplifying the parameters in advance, six equations cannot be solved for seven unknowns. In this paper, a rice height solution algorithm based on the OVoG model is implemented by solving the ground-phase first based on the characteristics of the rice growth scenario. The main steps are as follows:

- (1) The ground-phase was solved using complex coherent plane fitting.
- (2) A Genetic Algorithm (GA) is employed to optimize additional parameters by augmenting the observation quantity by utilizing multi-baseline data.

The radar response of rice is mainly determined by backward scattering from ground-volume interactions. As the underlying surface beneath rice is water, which has a very low backscattering coefficient, the primary scattering mechanism in rice growth scenarios is the ground-volume interaction and an accurate estimate of the topography can be obtained by exploiting this characteristic. Therefore, complex coherence coefficient point fitting was used to solve for the surface phase.

Based on the PolInSAR data obtained from the experiments, eight complex coherence points were calculated and plotted on a complex plane. A least-squares linear fitting method was used to fit the distributed complex coherence points to a coherent line. This line intersects with the unit circle at two points [23]. The narrower and longer the coherent

area formed by the distribution of the complex coherence points on the complex plane, the smaller the error of the linear fit [28]. Equation (3) can thus be expressed as follows:

$$\gamma_{\text{OVoG}}(\vec{\omega}) = e^{i\phi_0} \frac{\gamma_{\text{OV}}(\vec{\omega}) + \mu(\vec{\omega})}{1 + \mu(\vec{\omega})} = e^{i\phi_0} \left[\gamma_{\text{OV}}(\vec{\omega}) + \frac{\mu(\vec{\omega})}{1 + \mu(\vec{\omega})} (1 - \gamma_{\text{OV}}(\vec{\omega})) \right] \quad (7)$$

When the ground volume ratio $\mu(\vec{\omega})$ equals zero, the value of $\gamma_{\text{OVoG}}(\vec{\omega})$ is equivalent to the volume scattering correlation coefficient $e^{i\phi_0} \gamma_{\text{OV}}(\vec{\omega})$. As $\mu(\vec{\omega})$ approaches infinity, the value of $\gamma_{\text{OVoG}}(\vec{\omega})$ represents pure ground scattering $e^{i\phi_0}$. The range of values according to the formula lies between $e^{i\phi_0} \gamma_{\text{OV}}(\vec{\omega})$ and $e^{i\phi_0}$. It is determined that the two intersection points of the linear fit derived from complex coherence points with the complex unit circle correspond to the values $e^{i\phi_0} \gamma_{\text{OV}}(\vec{\omega})$ and $e^{i\phi_0}$, and identifying the value $e^{i\phi_0}$ allows for the determination of the ground-phase value ϕ_0 [29].

The preprocessed imaging center of the data used in this experiment was 0.65 m above the platform, which corresponds to a 0° phase angle (on the positive real axis) in the complex plane. The ground-phase point can be determined based on this feature. The fitted straight-line plot of the complex coherence coefficient for rice at 5.0 GHz is shown in Figure 4. The complex coherence points for the rice cluster on the complex plane and the fitted line intersect the unit circle in the first and fourth quadrants. A phase angle of $<0^\circ$ corresponds to a height below the imaging center, whereas the opposite is true for a height above the imaging center. Hence, an intersection point with a phase angle < 0 can be identified as the ground-phase point by computing the phase angles of the two intersection points.

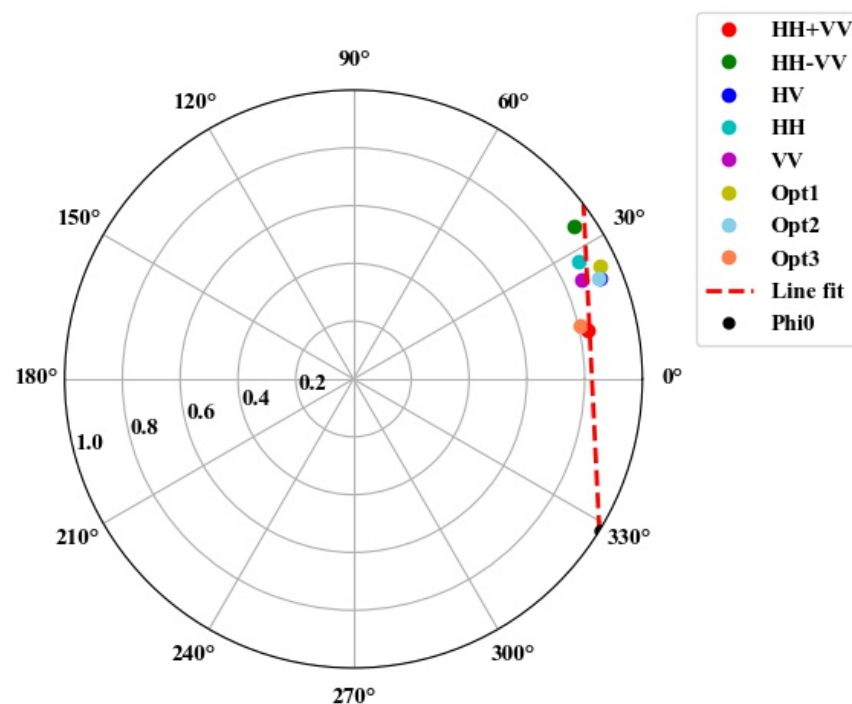


Figure 4. Two intersections of the fitted straight line with the complex plane at 5.0 GHz.

Genetic algorithms simulate the processes of biological inheritance and natural selection found in nature. These algorithms are designed to select the optimal parameter combinations to optimize an objective function. Genetic algorithms that mimic the mechanisms of biological evolution were developed since the biological processes of inheritance, variation, and natural selection are akin to the search for an optimal solution within a feasible space. Ultimately, a stochastic global search and optimization of algorithms have

evolved. The model-fitting scheme for solving OVoG parameters using genetic algorithms was achieved by minimizing the model correlation and the global distance between the data, and the algorithm was derived from the GENOCOP2 genetic algorithm developed by Michalewicz. et al. [30,31].

In the actual solution process, the ground-phase was taken as the input, and the other six parameters were solved. The algorithm performs a search within a feasible space, aiming to minimize the differences between the calculated and measured values of the complex coherence coefficients for the three polarized channels. The output consists of feasible solutions. The initial values for each parameter were set as random values, the search ranges for each parameter were defined based on empirical knowledge (Table 2), and the solution was solved for 100 inversions for each frequency point.

Table 2. Feasible parameter ranges for the genetic algorithm.

Parameters	Realm
h_V (m)	0.5–1.5
σ_a σ_b (dB/m)	0–3
μ_{HH} μ_{HV} μ_{VV}	0–8

The algorithm assigns values to each unknown parameter in the specified feasible domain, calculates the simulated value of the complex coherence coefficient according to the equation, and determines the difference between the measured and simulated values of the complex coherence coefficient. The solution is the optimal solution when the difference reaches its minimum value after many iterations.

$$\min \left\| \left(\operatorname{Re}(\gamma_{pq_{sim}}) - \operatorname{Re}(\gamma_{pq_{obs}}) \right) + \left(\operatorname{Im}(\gamma_{pq_{sim}}) - \operatorname{Im}(\gamma_{pq_{obs}}) \right) \right\| \quad (8)$$

where pq are the three polarimetric channels, HH, HV, and VV, respectively; $\gamma_{pq_{obs}}$ denotes the measured values of the complex coherence coefficients of the three polarimetric channels, obtained experimentally; and $\gamma_{pq_{sim}}$ indicates the simulated values of the complex coherence coefficients for the three polarization channels, obtained by the equation.

3. Results and Discussion

Based on the LAMP microwave anechoic chamber measurement data, the described research method was used to achieve rice height inversion, and an analysis was conducted to investigate the impact of various factors, such as the incidence angle, frequency band, baseline length, and baseline combination, on the accuracy. A root mean square deviation and a mean average deviation (MAE) were used as evaluation metrics for the algorithm.

3.1. Effect of Incidence Angle

Example measurements with a 0.25° baseline and data in the 0.8–18 GHz range were used to examine the influence of seven different incidence angles ranging from 15° to 75° on rice plant height retrieval accuracy to effectively analyze the impacts of different incidence angles on the accuracy of rice plant height retrieval. The estimated values for rice height and ground-phase height under the conditions of a 0.25° baseline, 0.8–18 GHz frequency range, and incidence angles ranging from 15° to 75° with a 10° interval are shown in Figure 5a–g.

Various polarized electromagnetic waves can effectively interact with the rice canopy and the underlying surface with a 35° incidence angle, allowing the reflected signals to better capture this information (Figure 5). The RMSE and MAE for the rice plant height retrieval were 0.1932 m and 0.1358 m, respectively. Furthermore, optimal retrieval performance was observed in the incidence angle range of 35° – 55° and frequency range of 10–17 GHz (X and Ku bands).

The accuracy of the surface phase height estimation in the high-frequency band (13 GHz) was poor when the incidence angle was $<35^\circ$. This indicates that the penetrating

ability of high-frequency electromagnetic waves is limited at smaller incident angles, and they cannot adequately reflect information from the underlying surface. The X-band band struggled to effectively estimate the surface phase height at a 15° incidence angle. In addition, there was a significant estimation error in the height of the Ku-band surface phase at a 25° incidence angle. However, the retrieval results of the lower-frequency bands still maintained a good level of accuracy at lower incidence angles. For example, the inversion MAE for the C-band was 0.1595 m at a 15° incidence angle, whereas the X-band inversion MAE was 0.1176 m at a 25° incidence angle.

The propagation path of the electromagnetic waves through the rice layer was longer at incidence angles of 55°, resulting in significant signal attenuation and a diminished ability to effectively reflect information from the underlying surface. The overall accuracy of the surface phase estimation was notably poor at a 65° incidence angle, indicating that the signal attenuation is substantial when the propagation path is extended.

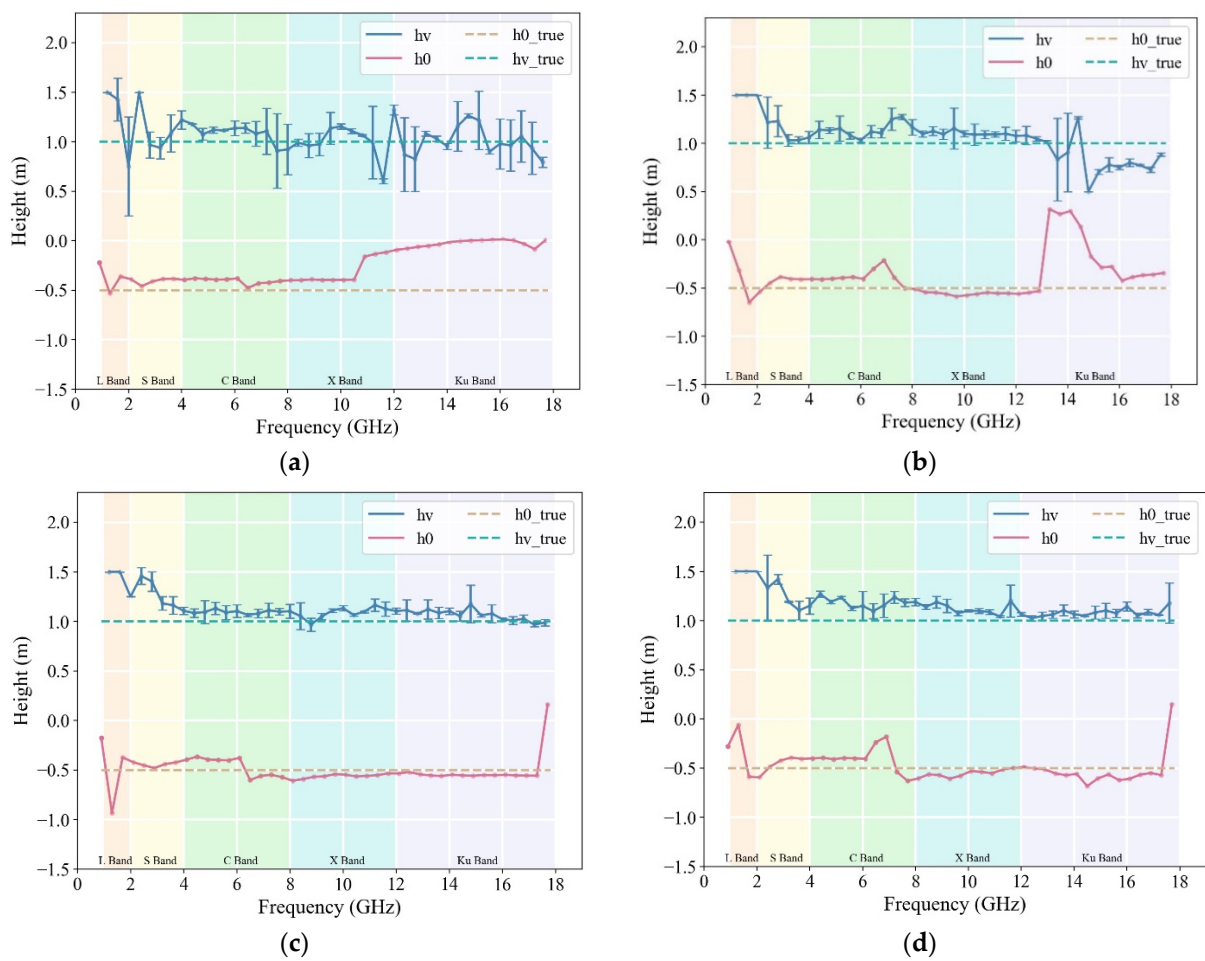


Figure 5. Cont.

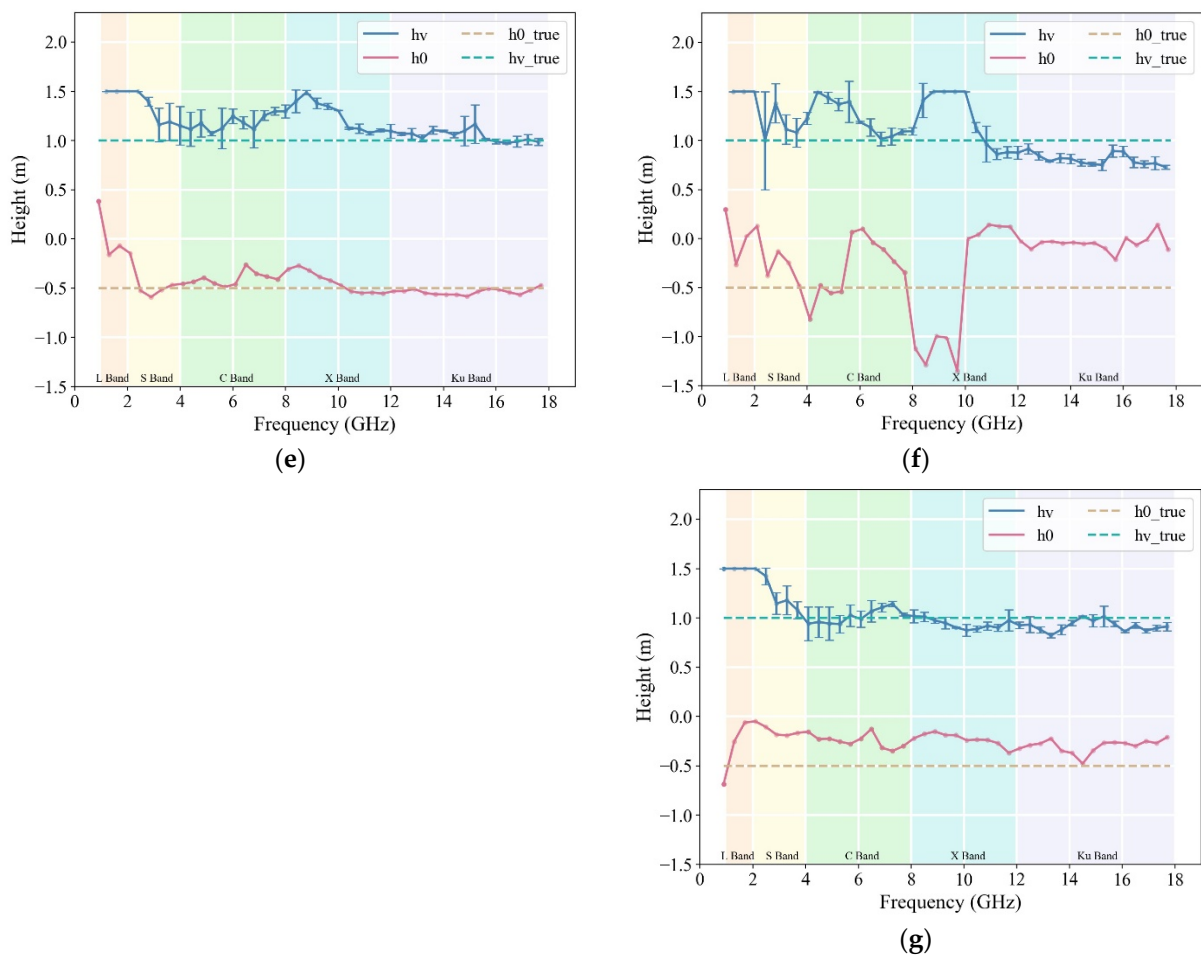


Figure 5. Inversion results for rice height at different incidence angles from 15° to 75° and continuous frequency bands from 0.8 to 18 GHz. (a) 15°; (b) 25°; (c) 35°; (d) 45°; (e) 55°; (f) 65°; (g) 75°.

The RMSE and MAE calculated for rice height estimates across different incidence angles (15–75°) within the 0.8–18 GHz frequency range are shown in Figure 6. The accuracy of rice plant height inversion initially increased with a greater incidence angle and then decreased with a larger incidence angle after 35°. The MAE for plant height estimation at a 35° incidence angle was the smallest, at 0.1359 m. The precision of vegetation height estimation was the lowest at a 65° incidence angle, with an RMSE of 0.3073 m and an MAE of 0.2598 m. This resulted in significant fluctuations in the estimated ground-phase. The advantage of the combined method lies in its ability to provide precise estimates of the ground-phase owing to the ground volume interaction of rice. However, the accuracy of the rice height estimation is compromised when there is a significant error between the estimated ground-phase values and the true values because the ground-phase serves as one of the input parameters for the optimization algorithm. Notably, the rice height estimation accuracy was relatively high at a 75° incidence angle, with an RMSE of approximately 0.1920 m and an MAE of approximately 0.1385 m. The highest accuracy for rice plant height inversion was obtained when the incidence angle of the radar data was 35–55° according to the analysis of rice plant height inversion results under different incidence angles.

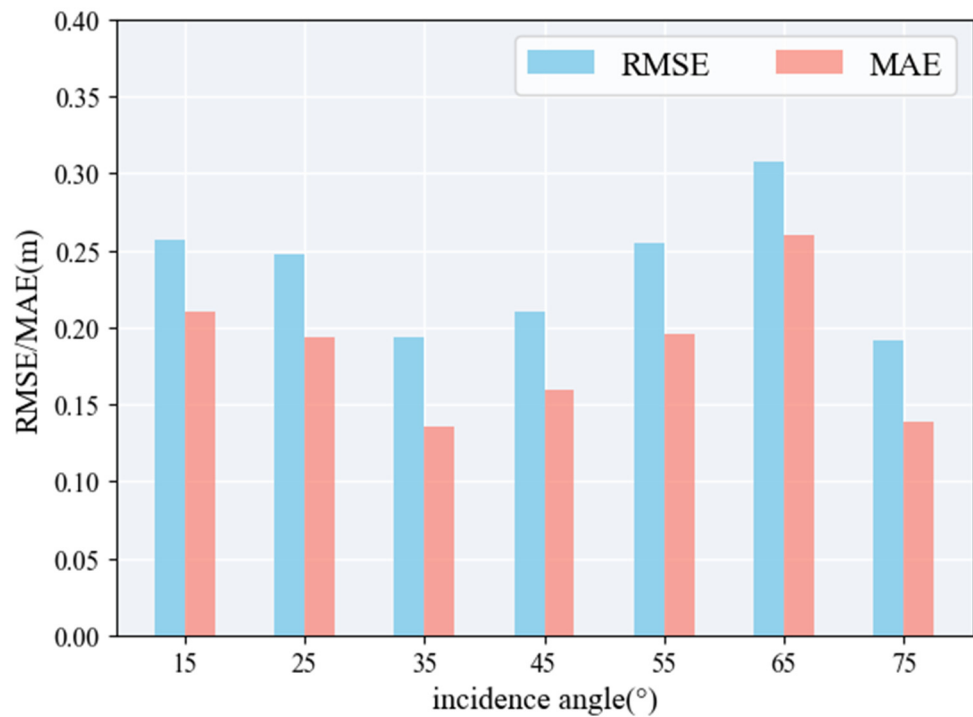


Figure 6. Root mean square deviation (RMSE) and mean average deviation (MAE) for rice height retrieval at 0.8–18 GHz under incidence angles ranging from 15° to 75°.

3.2. Effects of Baseline Length

Measurement data at a 45° incidence angle within the 0.8–18 GHz range were analyzed to effectively analyze the influence of different baseline lengths on the accuracy of rice plant height retrieval. The impacts of eight different baseline lengths, ranging from 0.25° to 2° were assessed at a 45° incidence angle. The estimated values for rice plant height and ground-phase height under the conditions described are shown in Figure 7a–g.

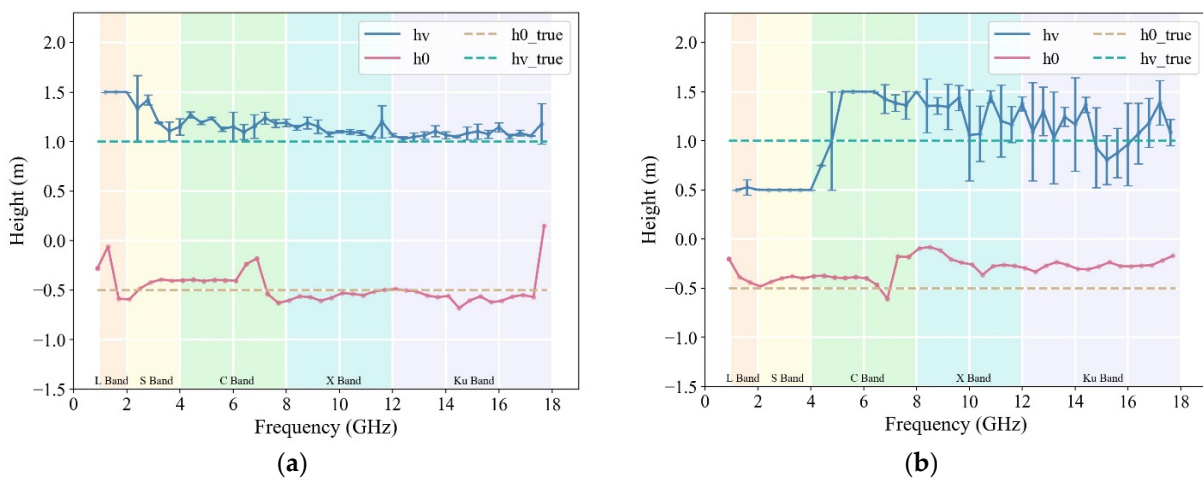


Figure 7. Cont.

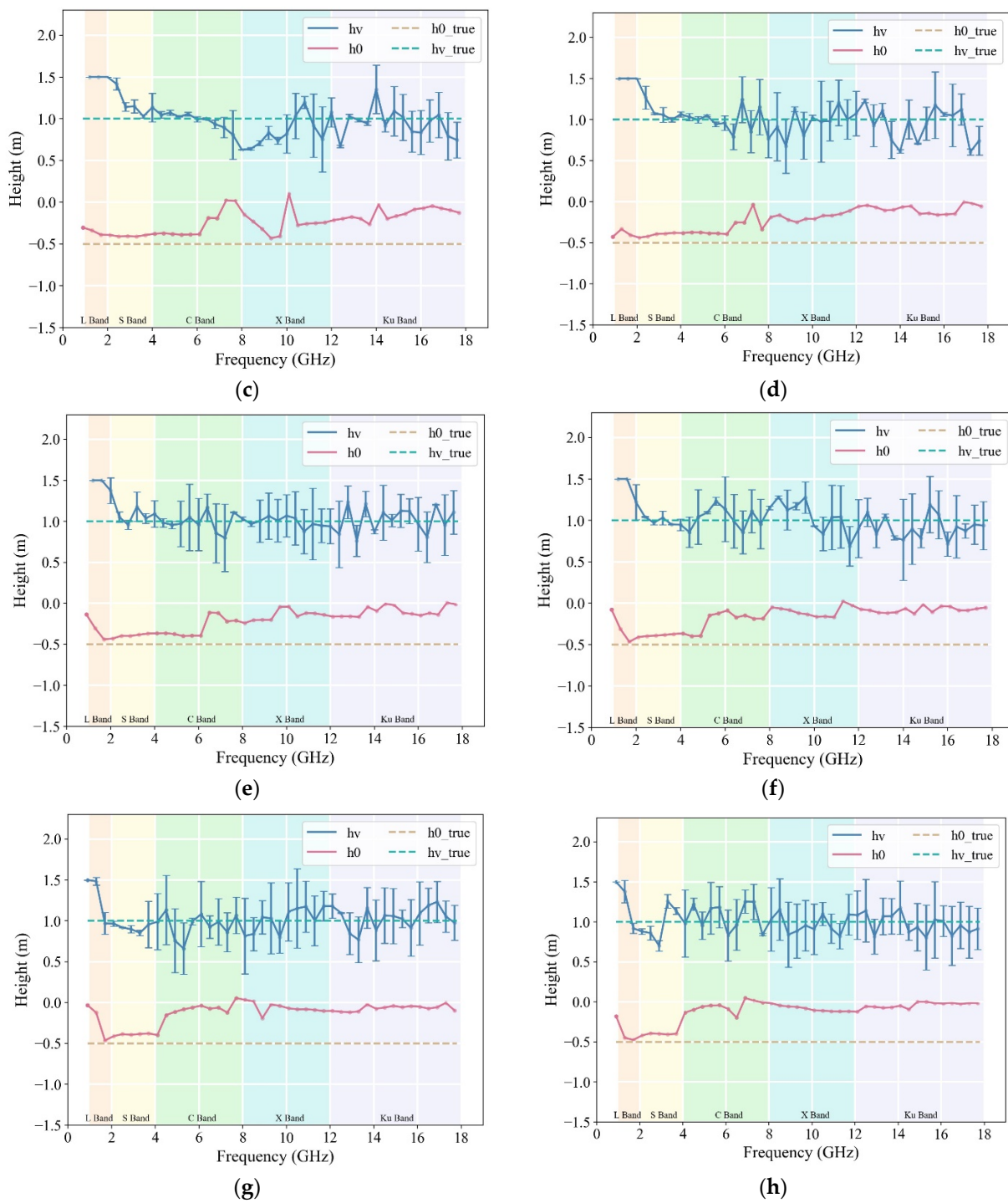


Figure 7. Inversion results for rice height for $B = 0.25^{\circ}$ – 2.0° baseline length at 45° incidence angle. (a) $B = 0.25^{\circ}$; (b) $B = 0.5^{\circ}$; (c) $B = 0.75^{\circ}$; (d) $B = 1.0^{\circ}$; (e) $B = 1.25^{\circ}$; (f) $B = 1.5^{\circ}$; (g) $B = 1.75^{\circ}$; (h) $B = 2.0^{\circ}$.

The best plant height inversion results were obtained with the 0.25° baseline condition, which showed good stability for all bands. The error between the estimated value of the surface phase and the true surface phase gradually increased as the baseline length increased, and the accuracy of the inversion results started to decrease in short-wave bands such as X and Ku, whereas more accurate rice plant heights could still be obtained in the C and S bands. The coherence of the PolInSAR data decreased when $B > 1.0^{\circ}$. The stability of the inversion results for the C- and S-bands deteriorated, and accurate plant height inversion results could not be obtained in the whole frequency band from 0.8 to 18 GHz.

The slope difference of the boundary line defining the coherent region is not a monotonic function of the baseline but shows fluctuations similar to a sine function and reaches zero for some baselines [32]. It is necessary to use relatively long baselines to increase the sensitivity in the vertical structure of the vegetation when using the PolInSAR data for rice height inversion. However, the process of the baseline increase is somewhat limited as the spectral shifts exceed the bandwidth at a certain length, resulting in decorrelation and a decrease in coherence to the extent of becoming zero.

The RMSE and MAE of the rice height estimates calculated in the frequency range of 0.8–18 GHz for the baseline length of 0.25–2.0° are shown in Figure 8. The values of the RMSE and MAE at $B = 0.25^\circ$ are both minimized to 0.1932 m and 0.1359 m, respectively, at an incidence angle of 45° , and the curves representing the ground-phase and vegetation height exhibited relatively stable variations. The ground-phase curve experienced notable fluctuations at $B = 0.5^\circ$, and the plant height followed a similar trend, resulting in decreased accuracy with RMSE and MAE values of 0.2620 m and 0.2071 m, respectively. The RMSE and MAE approached approximately 0.3 m and 0.25 m, respectively, and exhibited a generally positive correlation with baseline length when $B > 0.5^\circ$. Overall, the 0.25° baseline was the most suitable for rice height estimation. However, the selection of the optimal baseline length must consider the shape and structure of the target being measured. Research [21,33] on baseline lengths for forest height estimation suggests that shorter baselines can provide sufficient coherence for PolInSAR in terms of forest height retrieval owing to the higher average height of forests when compared with crops.

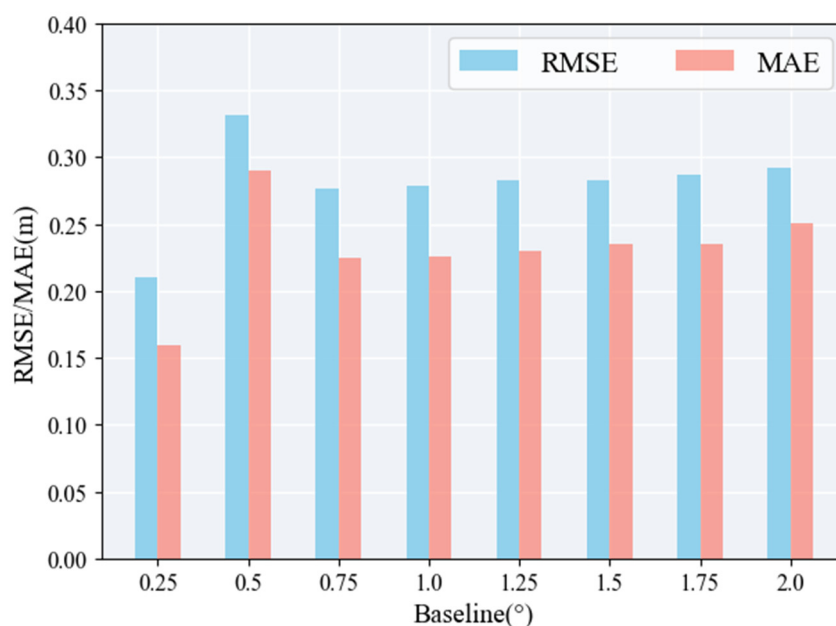


Figure 8. Root mean square deviation (RMSE) and mean average deviation (MAE) for rice height inversion at 0.25° – 2.0° baselines.

3.3. Effect of Baseline Combinations

3.3.1. Combination of Baselines with the Same Length

The effects of combining baselines of the same length on the inversion accuracy of rice height were analyzed at lengths of 0.25° and 0.5° , taking the 45° incidence angle and 0.8–18 GHz measurement data as an example. The estimated values of the rice height and ground-phase height under these conditions and incidence angles ranging from 15° to 75° are shown in Figures 9a–h and 10a–g.

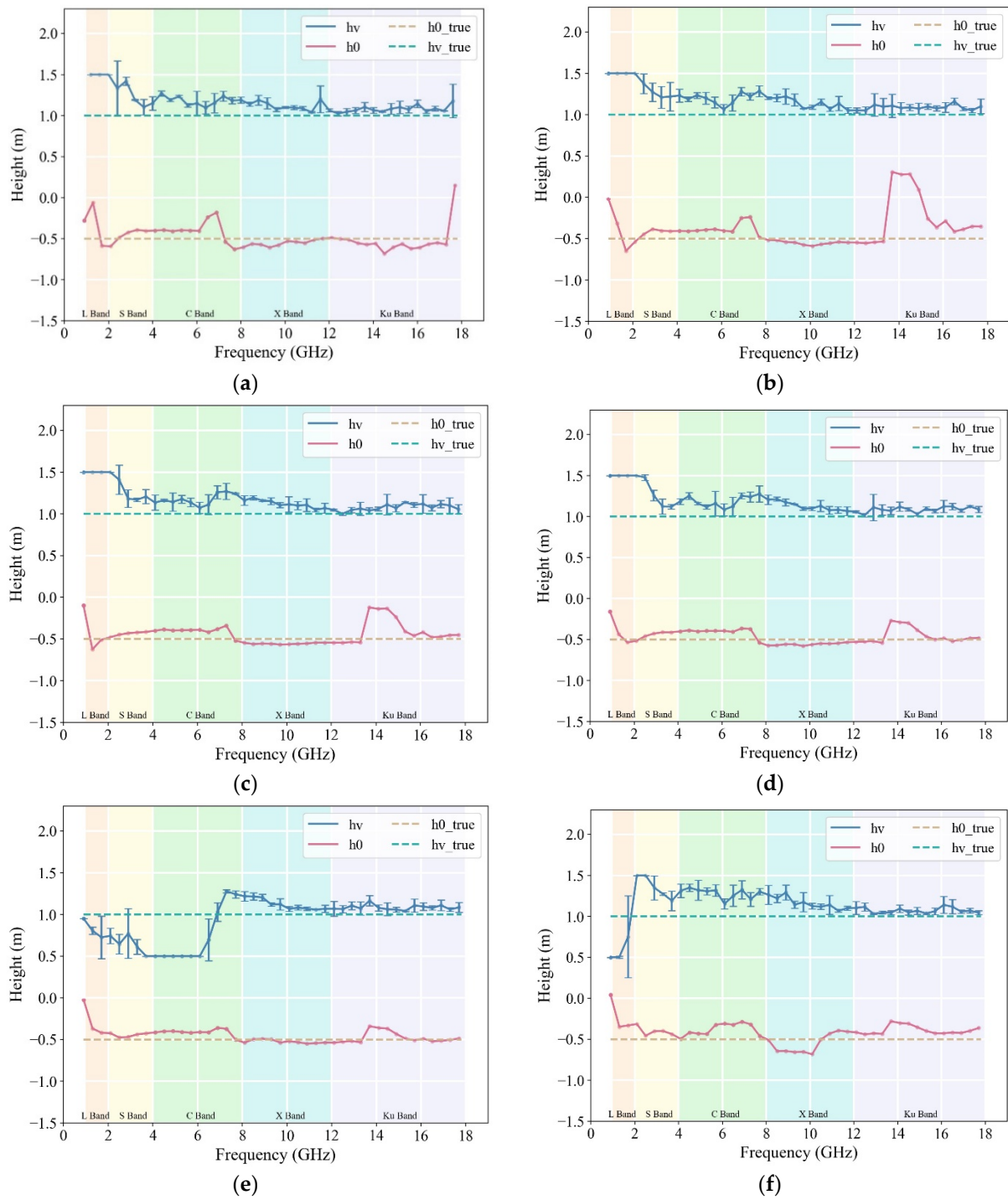


Figure 9. Cont.

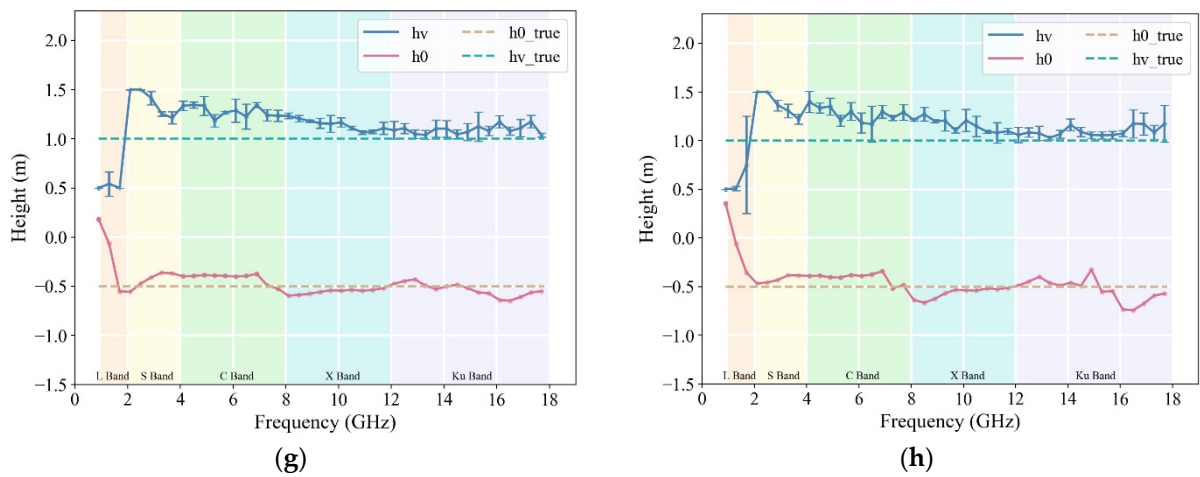


Figure 9. Vegetation height estimation for 0.25° 1–8 baseline combinations. (a) $B = 1$; (b) $B = 2$; (c) $B = 3$; (d) $B = 4$; (e) $B = 5$; (f) $B = 6$; (g) $B = 7$; (h) $B = 8$.

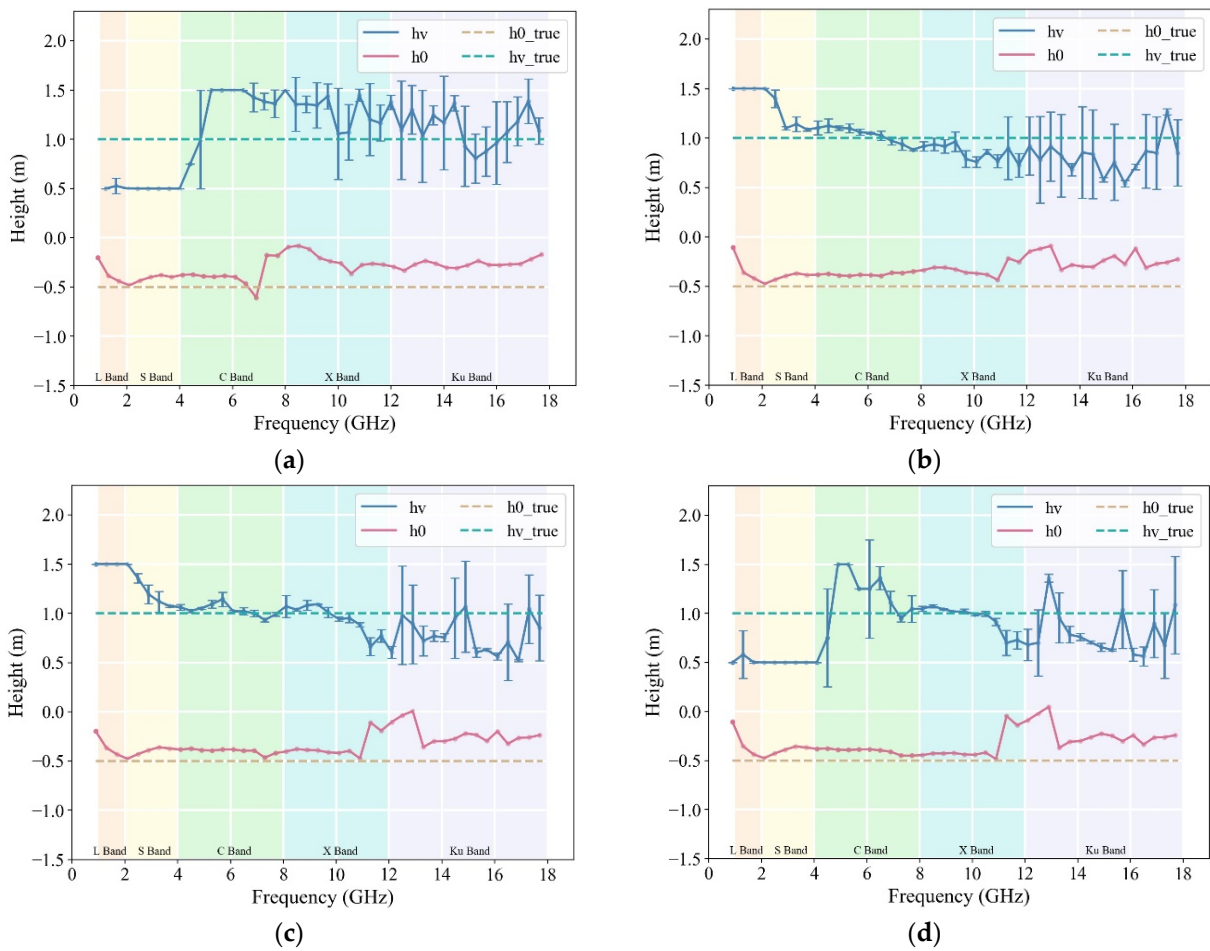


Figure 10. Cont.

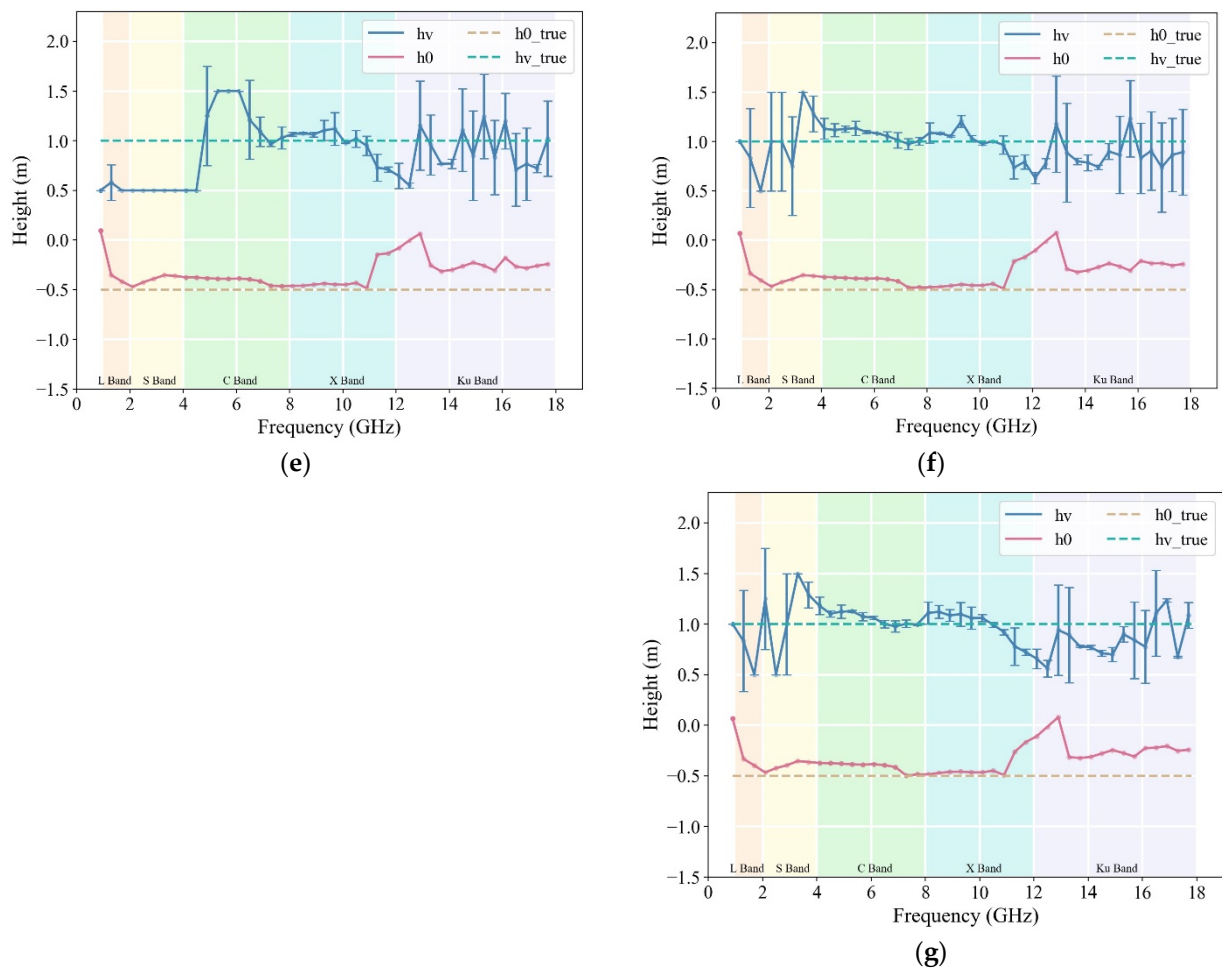


Figure 10. Vegetation height estimation at 0.5° and 1–7 baseline combinations. (a) $B = 1$; (b) $B = 2$; (c) $B = 3$; (d) $B = 4$; (e) $B = 5$; (f) $B = 6$; (g) $B = 7$.

Under the 0.25° baseline, combinations of one to four baselines yielded accurate rice height estimates in both the C- and Ku bands. The stability of the algorithm for rice height retrieval increased with an increase in the number of baselines. However, the rice height resulted in an L-band transition from overestimation to underestimation when five baselines were used, and there was a decrease in accuracy in the S- and C-bands. Obtaining accurate rice height estimates with one baseline becomes challenging under a 0.5° baseline. Combining two to three baselines results in a higher accuracy in rice height estimations within the C-band. The proportion of accurate rice height estimates shifted to the X-band with four to five baselines. Under six to seven baselines, the increased number of baselines expands the observation space, allowing for the C- and X-bands to achieve higher estimation accuracy.

The RMSE and MAE calculated for rice height estimations in the 0.8–18 GHz frequency range using the same baseline combinations under 0.25° and 0.5° baseline lengths are shown in Figures 11 and 12. When utilizing 0.25° multi-baseline combinations for rice height retrieval, the accuracy of plant height does not increase with the number of baselines; instead, it follows a trend of initially increasing and then decreasing. The highest accuracy was achieved with a combination of the three baselines, yielding an RMSE of 0.2094 m and an MAE of 0.1560 m. When five baselines were used, the RMSE and MAE values reached their maxima at 0.2669 m and 0.2019 m, respectively. Furthermore, the accuracy of the algorithm is superior with one to four baselines when compared with five to eight baselines.

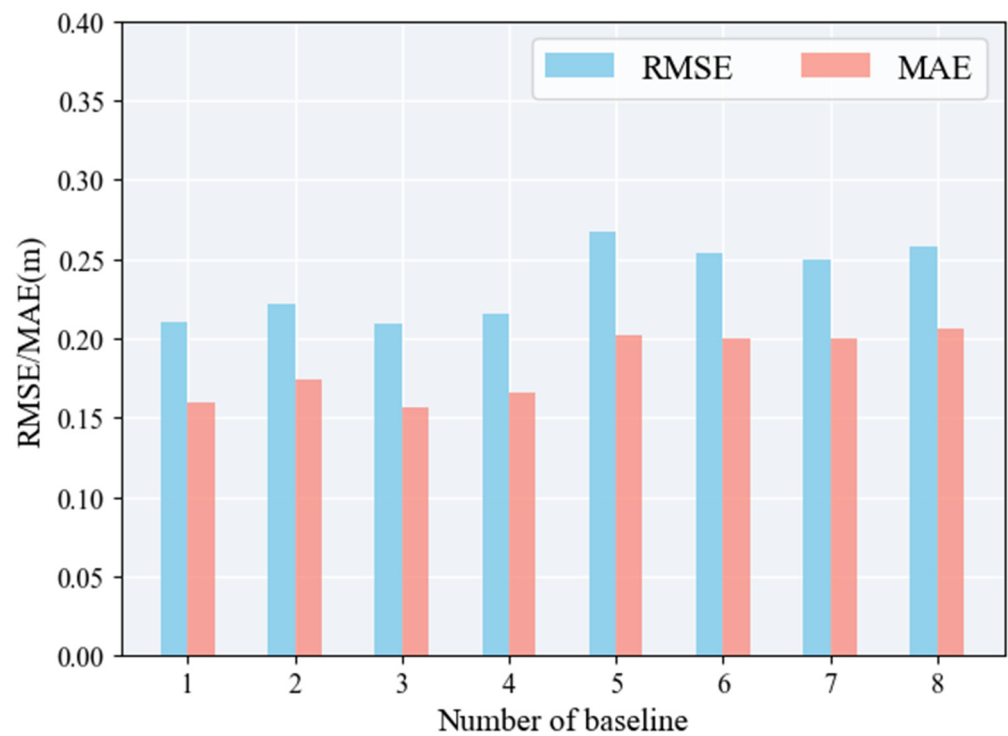


Figure 11. Root mean square deviation (RMSE) and mean average deviation (MAE) for rice height inversion at 0.25° same-length baseline combinations.

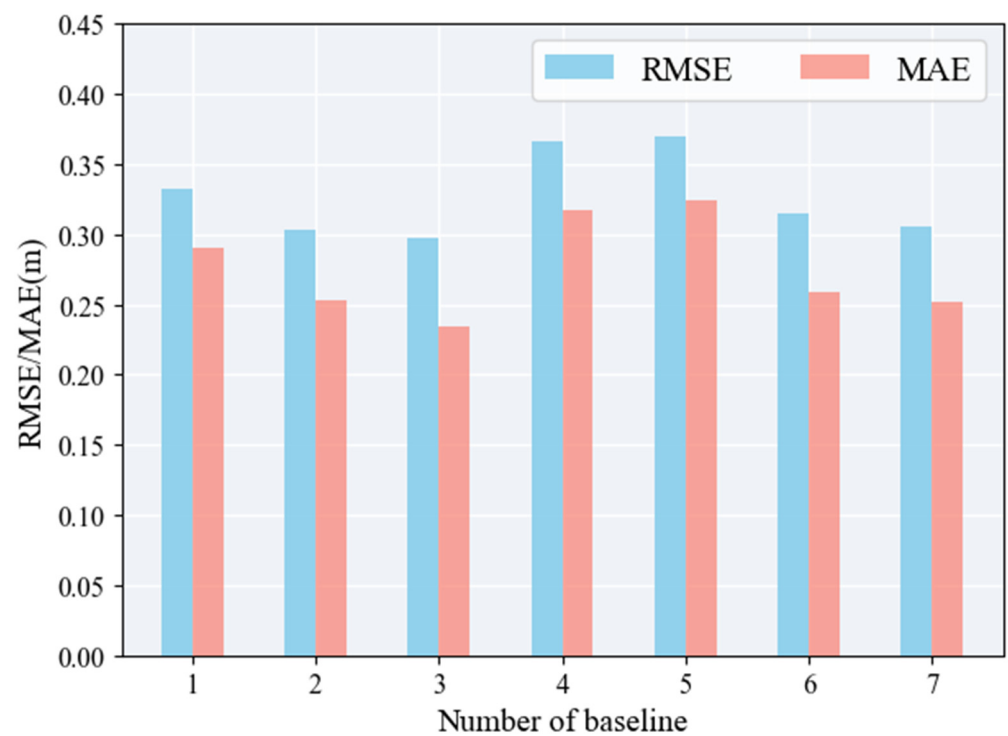


Figure 12. Root mean square deviation (RMSE) and mean average deviation (MAE) for rice height inversion at 0.5° same-length baseline combinations.

The rice height estimation results for 0.5° multi-baseline combinations exhibited the same trend as those for 0.25° (Figure 12). The highest accuracy was achieved with three baselines, with an RMSE of 0.2967 m and an MAE of 0.2340 m, whereas the accuracy decreased significantly when four baselines were used, and the worst accuracy were

achieved with five baselines. Within a certain range of baseline numbers, having more baselines of the same length can expand the observation space, reduce the variance and bias of the rice height estimation results, and enhance the stability of the retrieval outcomes. However, an excessive number of baselines limits the increased observation space, and a larger dataset may lead the algorithm to the local optima. Pichierri et al. [19] conducted Monte Carlo simulations to study the relationship between the number of baselines and the RMSE of corn height retrieval. They found that the RMSE negatively correlated with the number of baselines. However, further increases did not significantly reduce the estimation error when the number of baselines reached five. The conclusions drawn in this study regarding rice height retrieval and the number of baselines agree with Pichierri et al. [19].

3.3.2. Combination of Baselines with Different Lengths

The effect of the combination of baselines of different lengths on the inversion accuracy of rice height was analyzed with the 45° incidence angle and 0.8–18 GHz measurement data as examples. The 0.5° baseline was the base, and then successively increased by 0.75° , 1° , 1.25° , 1.5° , 1.75° , and 2° to analyze the effects of baseline combinations of different lengths on the accuracy of vegetation height inversion.

The RMSE and MAE calculated for different baseline combinations of rice height inversion based on the 0.5° baseline in the frequency range of 0.8–18 GHz are shown in Figure 13a–g. It is difficult to obtain accurate estimates of rice height using a 0.5° single baseline, and the accuracy improves in the S- and C-bands when three to four baselines are used for inversion. The accuracy of the rice height inversion was further improved in the X- and Ku-bands as the number of baselines increased from five to seven.

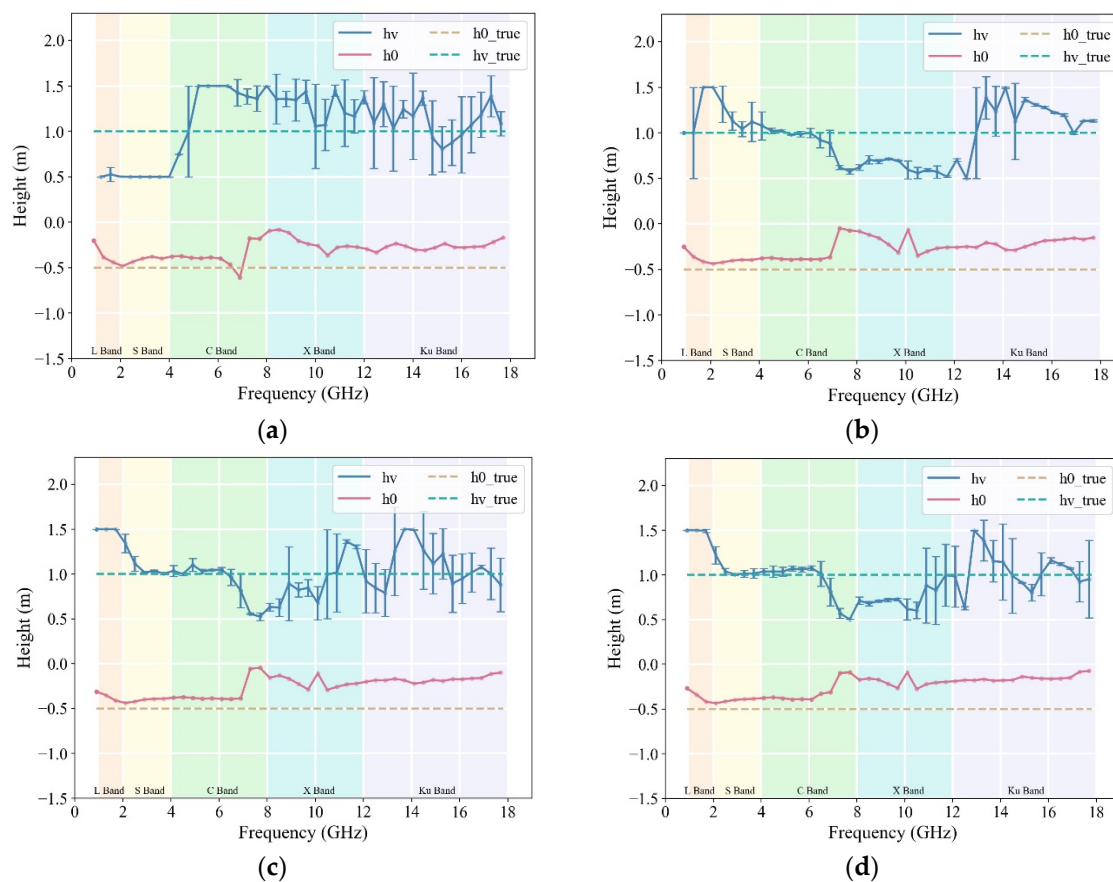


Figure 13. Cont.

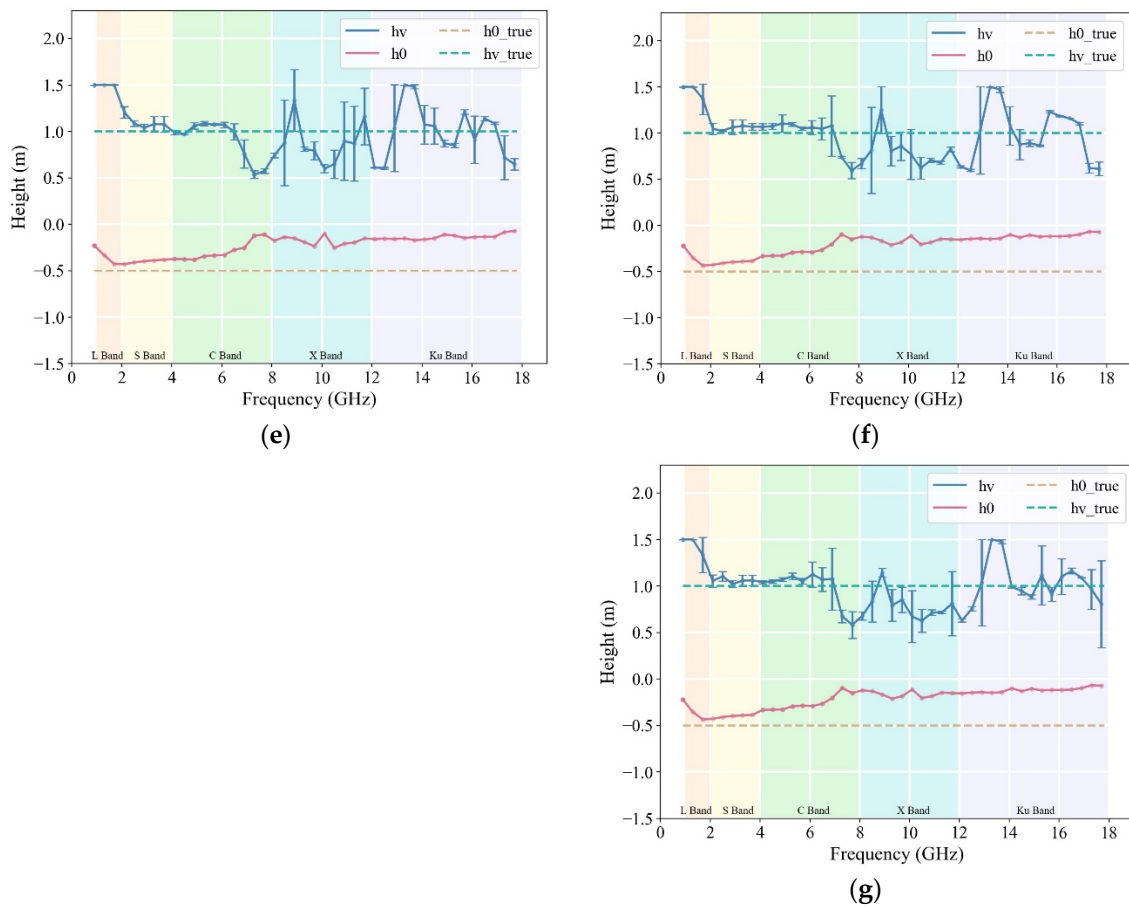


Figure 13. Vegetation height estimation for 0.5° at 1–7 different baseline combinations. (a) $B = 1$; (b) $B = 2$; (c) $B = 3$; (d) $B = 4$; (e) $B = 5$; (f) $B = 6$; (g) $B = 7$.

The RMSE and MAE of the rice height estimates for combinations of different baseline lengths based on a 0.5° baseline over a frequency range of 0.8–18 GHz are shown in Figure 14. The accuracy of rice height estimates increased as the number of baselines increased for different combinations. The accuracy of rice height estimates was the poorest with two baselines, since the RMSE and MAE values were 0.3381 m and 0.2873 m, respectively. The accuracy of the rice height estimation was highest with seven baselines, with RMSE and MAE values of 0.2804 m and 0.2231 m, respectively. The RMSE and MAE increased by approximately 0.05 m and 0.03 m when the number of baselines increased from one to four. However, the RMSE and MAE only increased by approximately 0.01 m as the number of baselines increased from four to seven. Longer baselines with a $B > 1.5^\circ$ exhibit a less significant improvement in accuracy owing to reduced coherence. Different baseline combinations can enhance the accuracy of rice height retrieval by expanding the observation space. However, it is essential to carefully select the baselines added to the combinations to maintain accuracy.

3.4. Optimal Baseline Combinations

From the preceding analysis, it is evident that the optimal range for rice plant height retrieval occurs at incidence angles between 35° and 55° with a baseline of 0.25° . Three to four baselines resulted in the highest accuracy in rice plant height retrieval and were identified as the optimal baseline quantity. In pursuit of optimal system parameters for rice plant height inversion, a combination of the best baseline length, quantity, and incidence angle within the identified optimal ranges was selected to further optimize inversion performance.

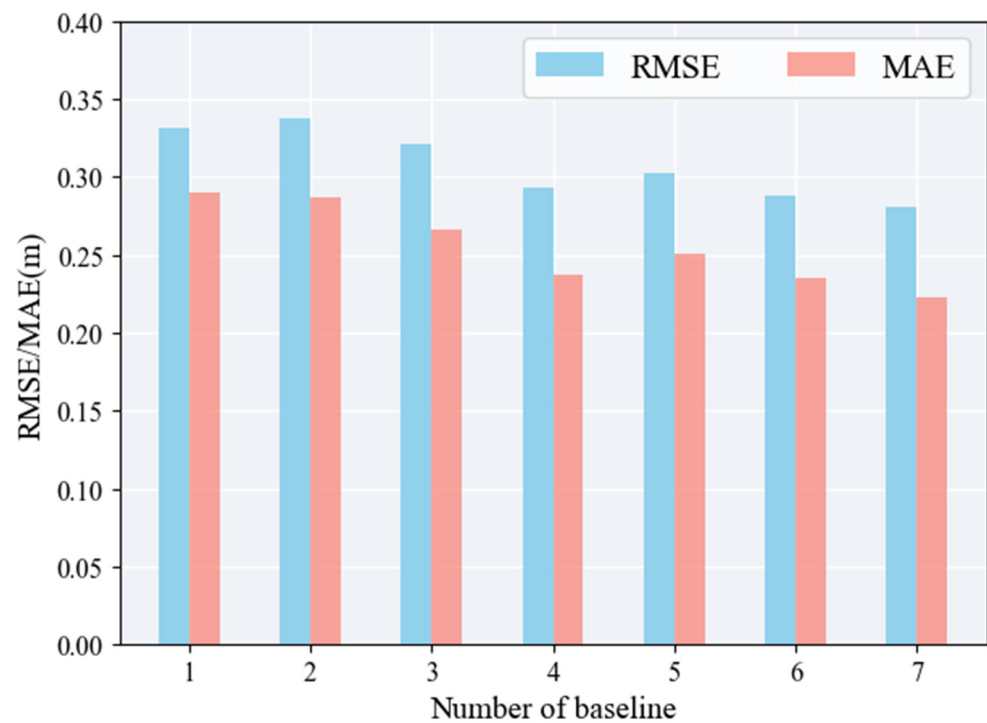


Figure 14. Root mean square deviation (RMSE) and mean average deviation (MAE) for inversion heights with different baseline algorithms added to the 0.5° baseline.

The first combination selected three baselines of 0.25° each at incidence angles of 35°, 45°, and 55° for the rice plant height inversion (Figure 15a). The curves of the surface phase and vegetation height inversion exhibited smooth profiles with a noticeable peak at approximately 6 GHz. The corresponding RMSE and MAE values were 0.2148 m and 0.1636 m, respectively, indicating a high level of accuracy in the inversion results. The second combination (building on the first) introduced an additional baseline of 0.5° at an incidence angle of 55°. The inversion results depicted in Figure 15b reveal an improved fit of the surface phase and vegetation height inversion curves to the ground truth. In particular, the error was less than 8 cm in the high-frequency portion > 7.5 GHz. The RMSE and MAE values were 0.1758 m and 0.1093 m, respectively, representing the highest accuracy among all the baseline combinations. This underscores the importance of selecting the preferred baseline combinations to improve the sensitivity of vegetation height retrieval algorithms to PolInSAR data.

In terms of selecting the incident wave frequency, the performance of the algorithm was relatively poor in the L-band and even in the lower frequency bands. Low-frequency waves exhibit strong penetration capabilities through vegetation, making it challenging to detect rich vertical information for low-lying crops. Short baseline data may result in overestimation of the S-band; however, the S-band can also achieve improved results with the selection of optimal baseline combinations. The C-, X-, and Ku-bands all exhibit strong retrieval capabilities and potential, making them the preferred frequency bands for the future retrieval of plant height for low-lying crops such as rice. These parameters can better facilitate the retrieval of vertical structural parameters, including plant height, for low-lying crops such as rice when combined with the optimal spatial baseline combinations proposed in this study.

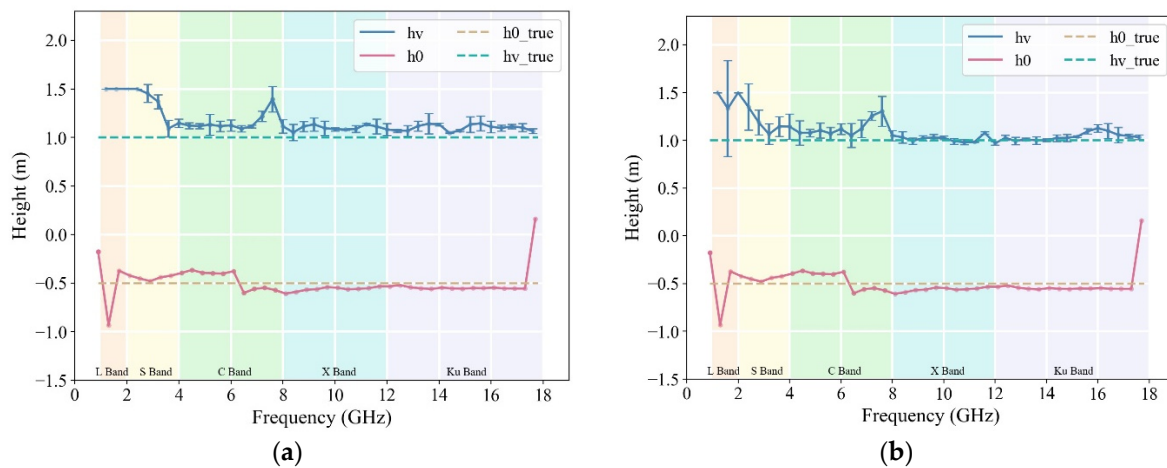


Figure 15. (a) Combinations of three baselines at 0.25° ; (b) combinations of three baselines at 0.25° each and one baseline at 0.5° at an incidence angle of 55° .

3.5. Equivalence Analysis of the LAMP Microwave Anechoic Chamber with On-Board SAR Imaging Geometry

The LAMP microwave anechoic chamber strives to simulate the imaging geometry of spaceborne SAR satellites to the greatest extent possible. However, certain differences still exist, primarily in imaging modes, signal acquisition, imaging principles, and other aspects. Therefore, equivalence must be considered to extend the research findings from the LAMP microwave anechoic chamber to practical applications in spaceborne SAR systems. Given the complexity of equivalence problems, this study focuses primarily on the simplest form of imaging geometry equivalence.

An equivalency analysis was conducted using imaging geometry from a domestically developed SAR satellite (GF-3 satellite) with polarimetric and interferometric measurement capabilities as an example. Building on this analysis, conclusions drawn from the LAMP microwave anechoic chamber were extended and applied to spaceborne SAR satellites. Specifically, an optimal detection mode for spaceborne SAR was proposed by focusing on rice height retrieval. This study provides a scientific basis for the design of future spaceborne SAR systems and their subsequent applications.

The slant distance of the LAMP microwave anechoic chamber is the distance from the dome antenna to the focus point of the platform, which is 9.3 m. However, in the actual experiment, the imaging position of the platform is 15 cm above the focus point of the platform, and according to the calculation, the actual slant distance should be 9.19 m. The orbital altitude of the GF-3 SAR satellite was 755 km, and the slant range of the GF-3 satellite was calculated based on the orbital altitude and incidence angle. By establishing the imaging geometry equivalence relationship between the LAMP microwave anechoic chamber and the GF-3 SAR satellite, the imaging geometry equivalence relationship between them can be constructed. The geometric equivalence relationship between the LAMP microwave anechoic chamber and the vertical baseline of the SAR satellite is as follows:

$$TB_n = S_T / S_L LB_n \quad (9)$$

where S_T and S_L denote the slant distances of the GF-3 satellite and the LAMP microwave anechoic chamber, respectively, and the TB_n and LB_n denote the vertical spatial baseline lengths corresponding to the interferometric measurements of the GF-3 satellite and the LAMP microwave anechoic chamber, respectively.

The spatial baseline of the LAMP microwave anechoic chamber was measured in terms of angles. In the actual calculations, the spatial baseline measured in degrees was first converted into a spatial baseline measured in units of distance. Geometric equivalency formulas were then used to establish the geometric spatial relationship between the LAMP

microwave anechoic chamber and the GF-3 satellite. When the incidence angle was 35° , the optimal spatial baseline lengths for the LAMP microwave anechoic chamber were calculated to be 0.25° and 0.50° , corresponding to the vertical spatial baseline lengths of the SAR GF-3 satellite system, as shown in Table 3.

Table 3. Geometric transformations of the LAMP microwave anechoic chamber and GF-3 SAR satellites.

Spatial Baseline	LAMP Anechoic Chamber		GF-3 SAR Satellite	
	Slope Distance (m)	Vertical Space Baseline (m)	Slope Distance (km)	Vertical Spatial Baseline (km)
0.25°	9.19	0.0401	921.68	4.07
0.50°	9.19	0.0802	921.68	8.14

Vertical wavenumber k_z is an important parameter for rice height inversion, and its magnitude is closely related to the PolInSAR retrieval of vegetation height. When k_z is excessively large, the coherence of PolInSAR decreases, leading to the risk of oversaturation in vegetation height retrieval, where heights above a certain threshold are underestimated. On the other hand, when k_z is too small, the sensitivity to the vertical structure of vegetation is reduced, making the height retrieval process susceptible to errors resulting from parameter variations. Different types of vegetation have specific ranges of vertical wave numbers that correspond to optimal PolInSAR measurement modes. By using measurement modes within these ranges, higher-precision vegetation height retrieval results can be obtained for vegetation of the respective type and height.

In the LAMP microwave anechoic chamber, the baseline vertical wave number was represented using the incidence angles. In spaceborne SAR systems, this baseline can be expressed in terms of the vertical spatial baseline length, where λ represents the wavelength of the incident wave, B_n is the interferometric vertical spatial baseline, R is the slant range from the antenna to the target, and θ is the incidence angle of the main interferometric image.

$$k_z = \frac{4\pi B_n}{\lambda R \sin\theta} \quad (10)$$

Based on the optimal incidence angle of $35\text{--}55^\circ$ and an optimal baseline length of 0.25° , the vertical wavenumber under the optimal baseline combination was calculated from the derived conclusions (Table 4), and the minimum value of the vertical wavenumber was 1.04, with a maximum value of 4.05.

Table 4. Range of k_z corresponding to the optimal baselines.

Length of Spatial Baseline ($^\circ$)	Angle of Incidence ($^\circ$)	Optimal Inversion Frequency Range for Rice Plant Height (GHz)	Range of k_z
0.25	35	4–18	1.04–4.05
	45	8–16	2.05–4.11
	55	9–18	1.99–3.98

Cloude and Papathanassiou [34] proposed to use the product of the vertical wave number and the vegetation height to $k_v = k_z h_v / 2$ to describe the optimal range of vegetation height inversion [12]. Based on the range of k_z obtained during the experimental process, an example is provided using a 35° incidence angle and a GF-3 satellite orbit height of 755 km to establish the functional relationship between B_n / λ and h_v (Figure 16). The two curves represent the upper and lower limits of the normal baseline wavelength ratio calculated based on the maximum k_{zmax} and minimum k_{zmin} of the vertical wavenumber, and the design of the spaceborne SAR will also be subject to the ratio B_n / λ which must be contained within the region plotted in Figure 16. The range of B_n / λ is 0.44–1.93 for the previously studied rice field with a height of 1 m.

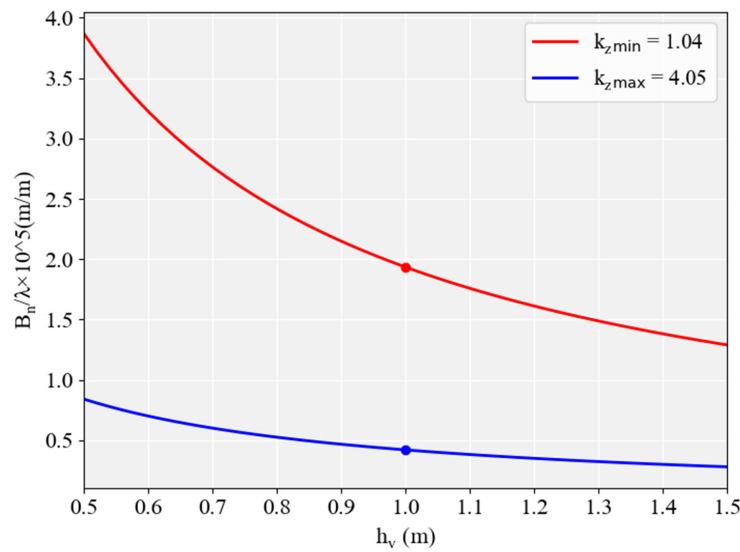


Figure 16. Normal baseline-to-wavelength ratio as a function of rice height.

Fixing the slant distance parameter R at 921.68 km and a baseline length of 0.25° gives two curves of the optimal vertical spatial baseline length versus frequency based on the minimum and maximum values of the optimal vertical wavenumber range, respectively (Figure 17). The red line indicates the maximum normal baseline for each frequency to avoid very low coherence, while the blue line indicates the minimum normal baseline to ensure sufficient volume sensitivity. In Figure 17, the center frequency points of the spaceborne SAR bands (S: 3.2 GHz, C: 5.3 GHz, X: 9.6 GHz, Ku: 15 GHz), the preferred ranges of vertical spatial baseline lengths are as follows: 4.10 to 15.97 km, 2.48 to 9.64 km, 1.36 to 5.32 km, and 0.87 to 3.40 km, respectively. The minimum vertical spatial baseline for the L-band (1.2 GHz) is 10.93 km, while the maximum spatial baseline, which is excessively large (42.59 km), is not displayed in the graph. In this case, the upper limits of the baseline corresponding to the minimum coherence also correspond to a very high normal baseline, which may be completely out of coherence in reality, and the lower limit restriction of the baseline is more relevant than the upper limit.

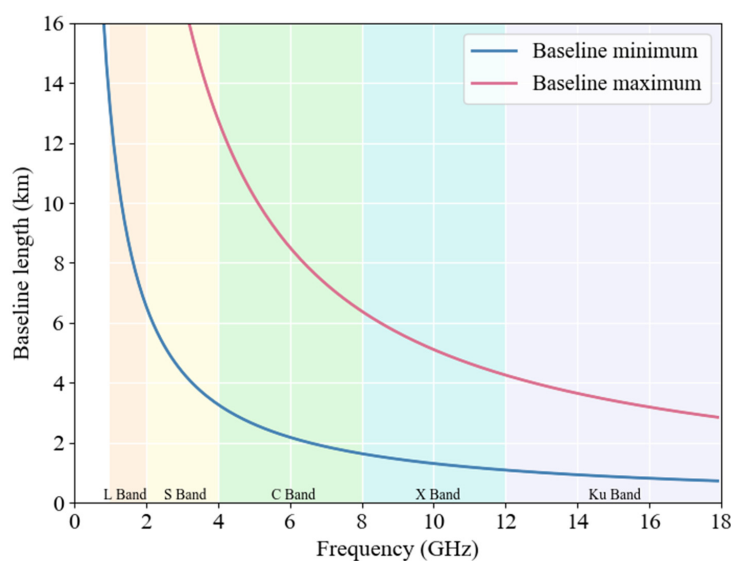


Figure 17. Variation curves for minimum and maximum vertical spatial baseline lengths with frequency.

4. Conclusions

In this study, a rice height inversion method based on the OVoG model was implemented using multi-frequency, multi-angle, and multi-baseline PolInSAR experimental data obtained from the LAMP microwave anechoic chamber. This study investigated the impact of changes in incident wave frequency, incident angle, and spatial baseline on the polarization interferometric response characteristics of rice, as well as their impact on the inversion results of rice height. Therefore, an optimal detection mode for PolInSAR interferometric measurements was proposed for rice height inversion.

The experiments demonstrate that the optimal incident angle range is 35° to 55° , with an optimal baseline length of 0.25° , yielding an RMSE of 0.1932 m and an MAE of approximately 0.1359 m, and the optimal frequency range is 4–16 GHz. For the number of baselines, a combination of 3 to 4, baselines were identified as the optimal number, with an RMSE of 0.1758 m and a MAE of approximately 0.1093 m.

Based on the equivalence of imaging geometries, the optimal spatial baseline ranges for the spaceborne SAR data on different frequency bands were: L-band: 10.93–42.59 km; S-band: 4.10–15.97 km; C-band: 2.48–9.64 km; and X-band: 1.36–5.32 km. Notably, the measurement modes corresponding to the C, X, and Ku bands were more suitable for PolInSAR rice height inversion.

Our future studies will continue to conduct theoretical and experimental research and expand the algorithm to different vegetation types. Additionally, we aim to verify the performance of the optimal detection mode by acquiring multi-temporal PolInSAR data using airborne SAR data, with the hope of providing a reliable basis for the design and preliminary research of a new generation of Earth observation SAR systems.

Author Contributions: B.Z. developed the algorithm of rice height inversion using multi-baseline PolInSAR measurements and analyzed the optimal detection baseline combination; K.L. designed the experiments and developed the PolInSAR measurement data processing methods; F.Z. and Y.S. assisted in designing the article structure and conducting experiments; D.W. and L.L. assisted in obtaining experimental data. All authors have read and agreed to the published version of the manuscript.

Funding: This work was supported by the National Natural Science Foundation of China (41871272), the Common Application Support Platform for Land Observation Satellites of China's Civil Space Infrastructure (CASPLoS_CCSI), and the Major Projects of China High-resolution Earth Observation System (00-Y30B01-9001-22/23).

Data Availability Statement: Data are contained within the article.

Acknowledgments: The authors would like to thank the staff at the Laboratory of Target Microwave Properties, Deqing Academy of Satellite Applications, for their assistance in the completion of the experiments, as well as Juan M. Lopez-Sanchez and J. David Ballester-Berman from the University of Alicante for their guidance and assistance.

Conflicts of Interest: The authors declare no conflict of interest.

References

1. Hazell, P.; Pachauri, R.K. *Bioenergy and Agriculture: Promises and Challenges*; IFPRI: Washington, DC, USA, 2006; Volume 2020.
2. Motohka, T.; Nasahara, K.; Miyata, A.; Mano, M.; Tsuchida, S. Evaluation of optical satellite remote sensing for rice paddy phenology in monsoon Asia using a continuous in situ dataset. *Int. J. Remote Sens.* **2009**, *30*, 4343–4357. [[CrossRef](#)]
3. Gao, G.; Yao, L.; Li, W.; Zhang, L.; Zhang, M. Onboard Information Fusion for Multisatellite Collaborative Observation: Summary, challenges, and perspectives. *IEEE Geosci. Remote Sens. Mag.* **2023**, *11*, 40–59. [[CrossRef](#)]
4. Li, N.; Lopez-Sanchez, J.M.; Fu, H.; Zhu, J.; Han, W.; Xie, Q.; Hu, J.; Xie, Y. Rice Crop Height Inversion from TanDEM-X PolInSAR Data Using the RVoG Model Combined with the Logistic Growth Equation. *Remote Sens.* **2022**, *14*, 5109. [[CrossRef](#)]
5. Tian, G.; Li, H.; Jiang, Q.; Qiao, B.; Li, N.; Guo, Z.; Zhao, J.; Yang, H. An Automatic Method for Rice Mapping Based on Phenological Features with Sentinel-1 Time-Series Images. *Remote Sens.* **2023**, *15*, 2785. [[CrossRef](#)]
6. Zhu, J.; Fu, H.; Wang, C. Methods and Research Progress of Underlying Topography Estimation over Forest Areas by InSAR. *Geomat. Inf. Sci. Wuhan Univ.* **2018**, *43*, 2030–2038.
7. Zhang, W.; Chen, E.; Li, Z.; Zhao, L.; Ji, Y. Development of Forest Height Estimation Using InSAR/PolInSAR Technology. *Remote Sens. Technol. Appl.* **2018**, *32*, 983–997.

8. Villard, L.; Le Toan, T. Relating P-Band SAR Intensity to Biomass for Tropical Dense Forests in Hilly Terrain: γ^0 or t^0 ? *IEEE J. Sel. Top. Appl. Earth Obs. Remote Sens.* **2014**, *8*, 214–223. [[CrossRef](#)]
9. Neeff, T.; Dutra, L.V.; dos Santos, J.R.; Freitas, C.d.C.; Araujo, L.S. Tropical forest measurement by interferometric height modeling and P-band radar backscatter. *For. Sci.* **2005**, *51*, 585–594.
10. Praks, J.; Antropov, O.; Hallikainen, M.T. LIDAR-aided SAR interferometry studies in boreal forest: Scattering phase center and extinction coefficient at X-and L-band. *IEEE Trans. Geosci. Remote Sens.* **2012**, *50*, 3831–3843. [[CrossRef](#)]
11. Zheng-Shu, Z.; Cloude, S.R. The development of a ground based polarimetric SAR interferometer (GB-POLInSAR). In Proceedings of the 2005 IEEE International Geoscience and Remote Sensing Symposium, Seoul, Republic of Korea, 29 July 2005; pp. 1097–1100.
12. Cloude, S.R.; Papathanassiou, K.P. Polarimetric SAR interferometry. *IEEE Trans. Geosci. Remote Sens.* **1998**, *36*, 1551–1565. [[CrossRef](#)]
13. Treuhaft, R.N.; Siqueira, P.R. Vertical structure of vegetated land surfaces from interferometric and polarimetric radar. *Radio Sci.* **2000**, *35*, 141–177. [[CrossRef](#)]
14. Romero-Puig, N.; Lopez-Sanchez, J.M.; Busquier, M. Evaluation of PolInSAR Observables for Crop-Type Mapping Using Bistatic TanDEM-X Data. *IEEE Geosci. Remote Sens. Lett.* **2022**, *19*, 1–5. [[CrossRef](#)]
15. Xi, C.; Hong, Z.; Chao, W. The inversion of vegetation structural parameters using dual-baseline polarimetric SAR interferometry. *Remote Sens. Nat. Resour.* **2009**, *21*, 49–52.
16. Treuhaft, R.N.; Moghaddam, M.; van Zyl, J.J. Vegetation characteristics and underlying topography from interferometric radar. *Radio Sci.* **1996**, *31*, 1449–1485. [[CrossRef](#)]
17. Treuhaft, R.N.; Cloude, S.R. The structure of oriented vegetation from polarimetric interferometry. *IEEE Trans. Geosci. Remote Sens.* **1999**, *37*, 2620–2624. [[CrossRef](#)]
18. Romero-Puig, N.; Marino, A.; Lopez-Sanchez, J.M. Application of the Trace Coherence to HH-VV PolInSAR TanDEM-X Data for Vegetation Height Estimation. *IEEE Trans. Geosci. Remote Sens.* **2022**, *60*, 1–10. [[CrossRef](#)]
19. Pichierri, M.; Hajnsek, I.; Papathanassiou, K.P. A multibaseline Pol-InSAR inversion scheme for crop parameter estimation at different frequencies. *IEEE Trans. Geosci. Remote Sens.* **2016**, *54*, 4952–4970. [[CrossRef](#)]
20. Lopez-Sanchez, J.M.; Hajnsek, I.; Ballester-Berman, J.D. First demonstration of agriculture height retrieval with PolInSAR airborne data. *IEEE Geosci. Remote Sens. Lett.* **2011**, *9*, 242–246. [[CrossRef](#)]
21. Garestier, F.; Dubois-Fernandez, P.C.; Champion, I. Forest height inversion using high-resolution P-band Pol-InSAR data. *IEEE Trans. Geosci. Remote Sens.* **2008**, *46*, 3544–3559. [[CrossRef](#)]
22. Lopez-Sanchez, J.M.; Ballester-Berman, J.D. Model assessment and inversion limitations of polarimetric SAR interferometry applied to crop monitoring. In Proceedings of the 6th European Conference on Synthetic Aperture Radar (EUSAR), Dresden, Germany, 16–18 May 2006; pp. 16–18.
23. Ballester-Berman, J.D.; López-Sánchez, J.M.; Fortuny-Guasch, J. Retrieval of biophysical parameters of agricultural crops using polarimetric SAR interferometry. *IEEE Trans. Geosci. Remote Sens.* **2005**, *43*, 683–694. [[CrossRef](#)]
24. Li, K.; Shao, Y.; Wang, J.; Wang, Z.; Guo, X.; Liu, X.; Xiao, X.; Liu, Z.; Wu, X.; Hailin, E. Anechoic Chamber Polinsar Measurements of Rice Canopy. In Proceedings of the IGARSS 2022–2022 IEEE International Geoscience and Remote Sensing Symposium, Kuala Lumpur, Malaysia, 17–22 July 2022; pp. 5349–5352.
25. Liu, X.; Shao, Y.; Li, K.; Liu, Z.; Liu, L.; Xiao, X. Backscattering Statistics of Indoor Full-Polarization Scatterometric and Synthetic Aperture Radar Measurements of a Rice Field. *Remote Sens.* **2023**, *15*, 965. [[CrossRef](#)]
26. Ballester-Berman, J.D.; Lopez-Sanchez, J.M. Combination of direct and double-bounce ground responses in the homogeneous oriented volume over ground model. *IEEE Geosci. Remote Sens. Lett.* **2010**, *8*, 54–58. [[CrossRef](#)]
27. Cloude, S.R. Dual-baseline coherence tomography. *IEEE Geosci. Remote Sens. Lett.* **2007**, *4*, 127–131. [[CrossRef](#)]
28. Ungria, E.; Ballester-Berman, J.D.; Lopez-Sanchez, J.M. Quality Assessment of the Oriented Volume over Ground (OVog) Model for POLInSAR Retrieval Algorithms Applied to Agricultural Crops. In Proceedings of the 2nd International Workshop POLINSAR 2005 (ESA SP-586), Frascati, Italy, 17–21 January 2005; Lacoste, H., Ed.; p. 13, ISBN 92-9092-897-2.
29. Cloude, S.; Papathanassiou, K. Three-stage inversion process for polarimetric SAR interferometry. *IEEE Proc. Radar Sonar Navig.* **2003**, *150*, 125–134. [[CrossRef](#)]
30. Lopez-Sanchez, J.M.; Ballester-Berman, J.D.; Marquez-Moreno, Y. Model limitations and parameter-estimation methods for agricultural applications of polarimetric SAR interferometry. *IEEE Trans. Geosci. Remote Sens.* **2007**, *45*, 3481–3493. [[CrossRef](#)]
31. Michalewicz, Z.; Michalewicz, Z. Evolutionary programming and genetic programming. In *Genetic Algorithms+ Data Structures= Evolution Programs*; Springer: Berlin/Heidelberg, Germany, 1996; pp. 283–287.
32. Pichierri, M.; Hajnsek, I. Comparing performances of crop height inversion schemes from multifrequency pol-InSAR data. *IEEE J. Sel. Top. Appl. Earth Obs. Remote Sens.* **2017**, *10*, 1727–1741. [[CrossRef](#)]
33. Garestier, F.; Dubois-Fernandez, P.C.; Papathanassiou, K.P. Pine forest height inversion using single-pass X-band PolInSAR data. *IEEE Trans. Geosci. Remote Sens.* **2007**, *46*, 59–68. [[CrossRef](#)]
34. Cloude, S. *Polarisation: Applications in Remote Sensing*; Oxford University Press: Oxford, UK, 2009.

Disclaimer/Publisher’s Note: The statements, opinions and data contained in all publications are solely those of the individual author(s) and contributor(s) and not of MDPI and/or the editor(s). MDPI and/or the editor(s) disclaim responsibility for any injury to people or property resulting from any ideas, methods, instructions or products referred to in the content.